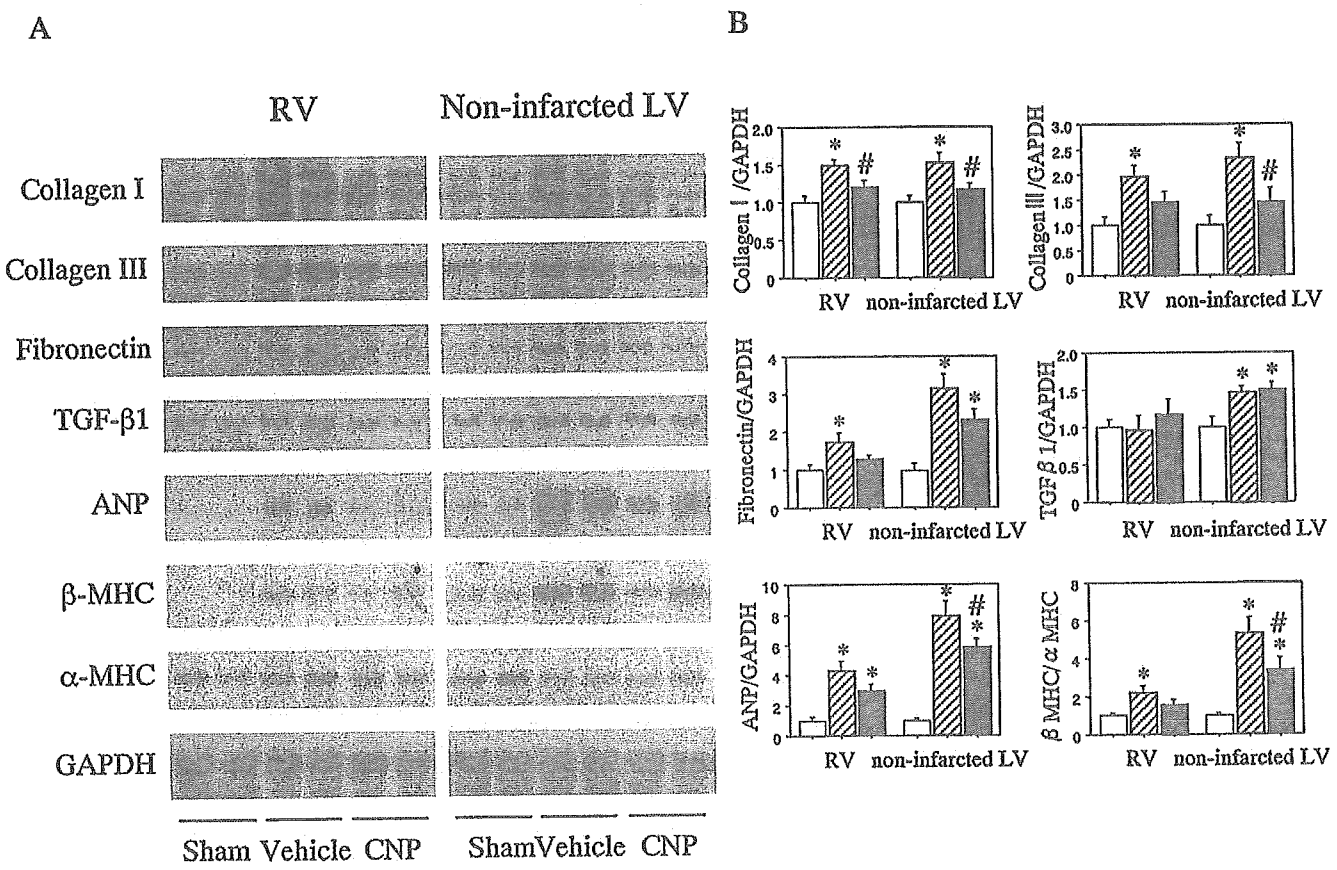

Figure 4. The effect of C-type natriuretic peptide (CNP) on messenger ribonucleic acid (mRNA) expression associated with cardiac remodeling after myocardial infarction (MI). **(A)** Typical autoradiograms of Northern blot analysis of mRNA levels in right ventricle (RV) and noninfarcted left ventricle (LV) for collagen type I, collagen type III, fibronectin, transforming growth factor-(TGF)-β-1, atrial natriuretic peptide (ANP), β- and α-myosin heavy chain (MHC), and glyceraldehyde-3-phosphate dehydrogenase (GAPDH) at the 18th day after MI. **(B)** Quantitative analyses of the abundance of each gene in the RV and noninfarcted LV at the 18th day after MI (n = 10 in each group). In individual samples, each mRNA value was corrected for the GAPDH mRNA value. Levels in sham-operated rats were arbitrarily assigned a value of 1.0. Values are mean ± SEM. $^{**}p < 0.01$, $^{*}p < 0.05$ compared with the sham-operated group; #$p < 0.05$ compared with the MI+vehicle group by analysis of variance and Bonferroni multiple-comparison *t* test. **Open bars** = sham; **striped bars** = MI+vehicle; **solid bars** = MI+CNP.

parameters in the infarcted LV between the two MI groups (data not shown).

Cellular mechanism of the antifibrotic action of CNP. C-type natriuretic peptide and 8-Bromo cGMP, an analog of cGMP, decreased the incorporation of [^{3}H]proline into cardiac fibroblasts in a dose-dependent manner (Figs. 5A and 5B). The decrease of [^{3}H]proline incorporation by CNP was completely blocked by Rp-8-pCPT-cGMP, a cell-permeable inhibitor of PKG type I and type II, at a concentration of 10^{-5} mol/l (Fig. 5C).

Endogenous CNP expression after MI. C-type natriuretic peptide mRNA expression increased on day 3 by about four-fold in the infarcted LV and two-fold in the noninfarcted LV compared with sham rats, and gradually decreased from day 7 to day 18 (Fig. 6A). C-type natriuretic peptide mRNA expression in RV slightly increased on day 7 only (1.5-fold) (Fig. 6A). In addition, immunohistochemical study revealed that CNP was stained mainly in fibrotic area of the infarct and border region on day 7 after MI (Fig. 6B). These results suggest that endogenous local CNP might play an important role in the infarcted heart.

DISCUSSION

In this study, we have demonstrated that in vivo administration of CNP improved cardiac function and protected against cardiac remodeling after MI in rats. The beneficial effects of CNP treatment in the heart after MI included attenuation of cardiac fibrosis, hypertrophy, and LV enlargement.

In addition, continuous treatment with CNP had no effects on mean arterial pressure and LV systolic pressure at the time of sacrifice 18 days after MI. The serial change in noninvasive blood pressure during the recovery period after MI was also similar in rats with and without CNP treatment. These findings are consistent with previous studies, which showed that CNP infusion had little vasodepressor or natriuretic activities in rats and healthy humans (4,11).

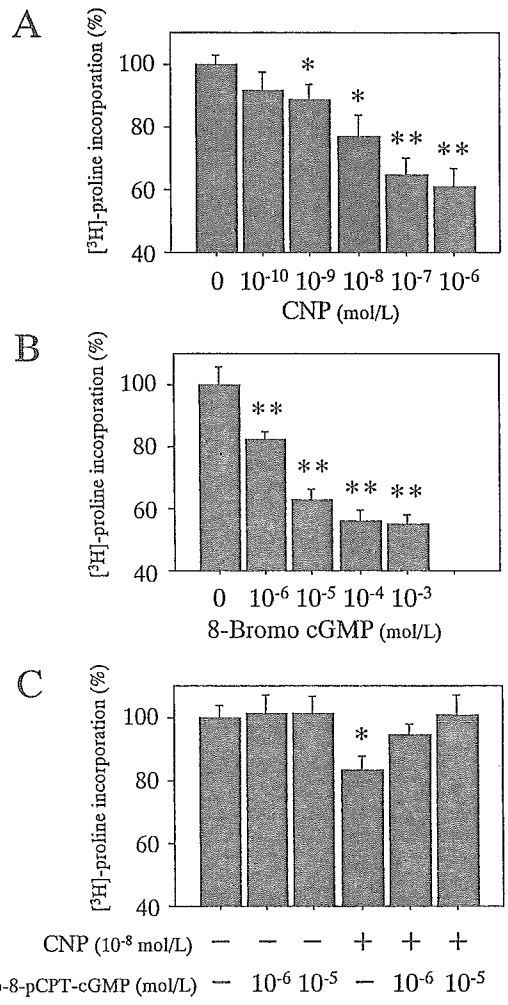

Figure 5. The effect of C-type natriuretic peptide (CNP) on collagen synthesis via the cyclic guanosine monophosphate (cGMP)/cyclic guanosine monophosphate-dependent protein kinase (PKG) pathway in cultured neonatal rat cardiac fibroblasts. **(A and B)** The effect of CNP and 8-Bromo cGMP on [^{3}H]proline incorporation in cardiac fibroblasts. **(C)** [^{3}H]proline incorporation in the presence or absence of 10^{-8} mol/l CNP with or without Rp-8-pCPT-cGMP, PKG inhibitor. Values are mean ± SEM. $^{**}p < 0.01$, $^{*}p < 0.05$ compared with control by analysis of variance and Bonferroni multiple-comparison *t* test.

Similarly, the heart rate was not significantly affected by CNP infusion throughout the study period.

The effect of CNP on cardiac performance. Chronic administration of CNP improved cardiac performance in MI rats, as indicated by increases in LV fractional shortening, cardiac output, and LV $dP/dt_{max/min}$, and by decreases in E/A ratio and LV end-diastolic pressure, which were accompanied by improvement of LV enlargement. Because the effect of CNP on pre- or after-load, heart rate, and infarct size was very little, a mechanism other than hemodynamic improvement or reduction in infarct size is probably the cause of the beneficial effects of CNP on cardiac performance.

The beneficial effect of CNP on cardiac remodeling through its antifibrotic action. One possibility is that CNP directly inhibits myocardial fibrosis because we have previously demonstrated that CNP directly inhibited both DNA and collagen synthesis by cardiac fibroblasts in vitro (6). In the present study, we have, therefore, examined the in vivo effect of CNP on fibrosis and found that CNP significantly attenuated an increase in morphometrical collagen volume fraction in the noninfarcted LV and RV. In addition, the effect of CNP was more prominent in the border region of MI, in which fibrosis was more increased, than that in the remote region. Because our preliminary study showed that a number of fibroblasts shift toward a myofibroblastic phenotype indicated by α-smooth muscle actin in the border region of MI, CNP might have more potent inhibitory effect on myofibroblast-like cells than on fibroblasts. Furthermore, the mRNA levels of collagen type I and III in the noninfarcted LV and RV were suppressed by treatment with CNP. These results provide in vivo evidence that CNP is a potent "fibrosis-inhibitory agent" after MI. The amount of myocardial collagen deposition in the infarcted and noninfarcted regions during healing after MI was reported to influence and to be integral to the process of ventricular remodeling (16). In addition, it has been shown that excessive accumulation of myocardial collagen might result in rigidity of the myocardium and severely impaired relaxation (17). Therefore, improved LV $dP/dt_{max/min}$ by CNP after MI might reflect improved myocardial rigidity in the noninfarcted region caused by the reduction in cardiac fibrosis.

Given the in vivo antifibrotic action of CNP, we further explored the cellular mechanisms of this action in vitro. Consistent with our previous study (6), CNP or 8-Bromo cGMP, an analog of cGMP, potently inhibited collagen synthesis of cultured cardiac fibroblasts. In the present study, the inhibitory effect of CNP was completely blocked by Rp-8-pCPT-cGMP, an inhibitor of PKG (Fig. 5), indicating that CNP inhibited collagen synthesis by activating cGMP/PKG pathway.

Some experimental data suggest that antifibrotic agents could potentially enhance the remodeling of the extracellular collagen matrix in the infarct zone during very early stage of healing after MI (18). However, in the present study, the death rate of the MI+CNP group (6%) was lower than that of the MI+vehicle group (17%) during the two-week infusion period, and two dead rats with CNP treatment showed no findings of LV rupture. The late start of CNP infusion at the fourth day of MI might reduce the potential adverse effects of antifibrosis such as wall thinning of infarct zone. Further studies are needed to determine the best timing of CNP treatment after MI.

The beneficial effect of CNP on cardiac remodeling through its antihypertrophic action. Another possible mechanism of cardioprotection by CNP might be attenuated myocardial hypertrophy after MI. As shown in the Results section, CNP effectively reduced the MI-induced myocardial hypertrophy in vivo. The findings are in agreement with previous in vitro studies, which showed that natriuretic peptides including CNP prevented hypertrophy

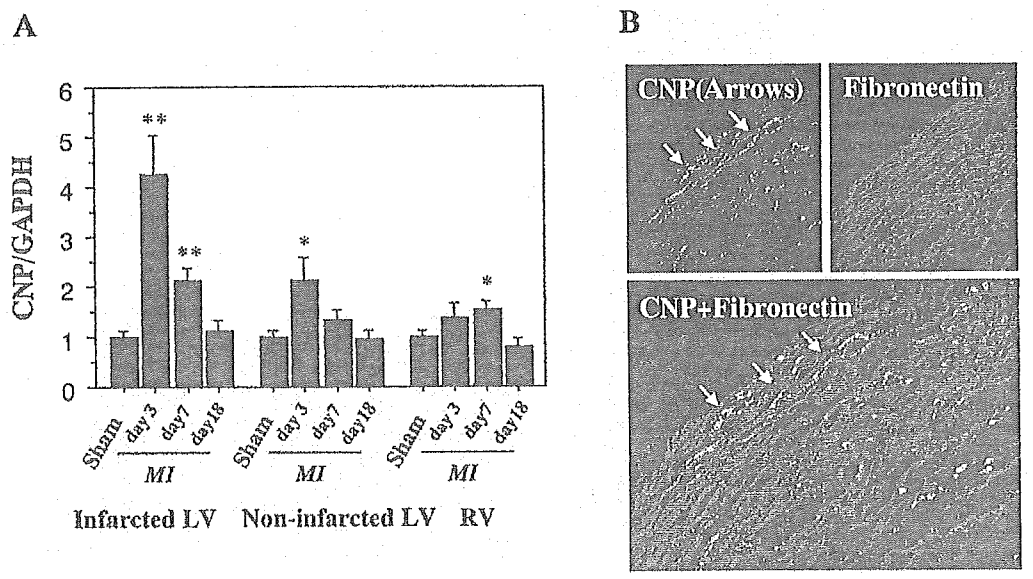

Figure 6. Endogenous C-type natriuretic peptide (CNP) expressions after myocardial infarction (MI). **(A)** Endogenous CNP mRNA abundance in the infarcted left ventricle (LV), noninfarcted LV, and right ventricle (RV) at different times after MI and on day 3 after sham operation. Values are mean ± SEM. $^{**}p < 0.01$, $^{*}p < 0.05$ compared with sham by analysis of variance and Bonferroni's multiple-comparison *t* test. **(B)** Immunofluorescent microscopic CNP expression. Upper photomicrographs show the section on day 7 after MI stained by the specific antibody against CNP-53 **(left, green)** and stained by antifibronectin antibody **(right, red)**. Lower photomicrograph shows the merged image (×600 magnification). GAPDH = glyceraldehydes-3-phosphate dehydrogenase.

of cultured cardiomyocytes (7,19). Although the precise mechanism by which CNP inhibits cardiac hypertrophy remains unknown, our previous study (7) suggested that CNP inhibits hypertrophy of cardiac myocytes directly by activating cGMP-dependent mechanism and indirectly by reducing endothelin-1 secretion from nonmyocytes.

On the other hand, because hypertrophy after MI is an adaptive response that offsets increased load, attenuates progressive dilation, and stabilizes contractile function (20), decreased cardiac hypertrophy shown in the present study might be caused by the indirect effect of CNP via decreased LV systolic wall stress. Further studies are needed to determine the contribution ratio of direct and indirect effects of CNP on cardiac hypertrophy.

Comparison with other antiremodeling therapies after MI. A number of therapeutic approaches to limiting ventricular remodeling in MI have been reported. These agents include angiotensin-converting enzyme inhibitors, angiotensin II type 1 receptor blockers, β-adrenergic blockers, aldosterone antagonists, and matrix metalloproteinase inhibitors. Although a number of these other agents have been given orally and, in this regard, they have an advantage over CNP, CNP treatment has some advantages concerning short treatment period and fewer side effects. Actually, in previous studies, it took more than four weeks for other agents to attain similar reduction of collagen volume fraction as two weeks treatment of CNP. Furthermore, these synthetic agents might cause harmful effects such as severe hypotension by vasodilators (21) or musculoskeletal toxicity by matrix metalloproteinase inhibitors (22). Because CNP does not affect blood pressure, it can be used in hemodynamically unstable patients as often seen in acute MI.

Study limitations. Because the effects of CNP were evaluated after two weeks of therapy in the present study, its long-term effects on the cardiac remodeling after MI remain unclear. For future clinical application, further study is necessary to examine if the antiremodeling effects of CNP persist for the long-term follow-up period.

Summary. Our study has demonstrated that continuous administration of CNP improved LV dysfunction and attenuated the development of cardiac remodeling after MI. Because CNP has much weaker vasorelaxant and natriuretic activities, but has much more potent antifibrotic and antihypertrophic actions than ANP or BNP, these beneficial effects of CNP might be associated with direct effects on the failing heart. In conclusion, CNP is potentially useful as a new antiremodeling agent through its novel mechanism of action.

Acknowledgments

The authors are grateful to Dr. Yujiro Hayashi, Daiichi Suntory Pharma, for the kind gift of CNP. We also thank Ms. Chika Fukuhara for her excellent technical assistance.

Reprint requests and correspondence: Dr. Ichiro Kishimoto, Department of Biochemistry, National Cardiovascular Center Research Institute, 5-7-1 Fujishiro-dai, Suita, Osaka 565-8565, Japan. E-mail: kishimot@ri.ncvc.go.jp.

REFERENCES

1. Rosenzweig A, Seidman CE. Atrial natriuretic factor and related peptide hormones. Annu Rev Biochem 1991;60:229–55.
2. Levin ER, Gardner DG, Samson WK. Natriuretic peptides. N Engl J Med 1998;339:321–8.

3. Nakao K, Ogawa Y, Suga S, et al. Molecular biology and biochemistry of the natriuretic peptide system. I: Natriuretic peptides. J Hypertens 1992;10:907–12.
4. Sudoh T, Minamino N, Kangawa K, Matsuo H. C-type natriuretic peptide (CNP): a new member of natriuretic peptide family identified in porcine brain. Biochem Biophys Res Commun 1990;168:863–70.
5. Furuya M, Miyazaki T, Honbou N, et al. C-type natriuretic peptide inhibits intimal thickening after vascular injury. Ann NY Acad Sci 1995;748:517–23.
6. Horio T, Tokudome T, Maki T, et al. Gene expression, secretion, and autocrine action of C-type natriuretic peptide in cultured adult rat cardiac fibroblasts. Endocrinology 2003;144:2279–84.
7. Tokudome T, Horio T, Soeki T, et al. Inhibitory effect of C-type natriuretic peptide (CNP) on cultured cardiac myocyte hypertrophy: interference between CNP and endothelin-1 signaling pathways. Endocrinology 2004;145:2131–40.
8. Kalra PR, Clague JR, Bolger AP, et al. Myocardial production of C-type natriuretic peptide in chronic heart failure. Circulation 2003; 107:571–3.
9. Hammermeister KE, DeRouen TA, Dodge HT. Variables predictive of survival in patients with coronary artery disease: selection by univariate and multivariate analysis from the clinical, electrocardiographic, exercise, arteriographic, and quantitative angiographic evaluations. Circulation 1979;59:421–30.
10. Sutton MG, Sharpe N. Left ventricular remodeling after myocardial infarction: pathophysiology and therapy. Circulation 2000;101: 2981–8.
11. Igaki T, Itoh H, Suga SI, et al. Effects of intravenously administered C-type natriuretic peptide in humans: comparison with atrial natriuretic peptide. Hypertens Res 1998;21:7–13.
12. Nagaya N, Uematsu M, Kojima M, et al. Chronic administration of ghrelin improves left ventricular dysfunction and attenuates development of cardiac cachexia in rats with heart failure. Circulation 2001;104:1430–5.
13. Fishbein MC, Maclean D, Maroko PR. Experimental myocardial infarction in the rat: qualitative and quantitative changes during pathologic evolution. Am J Pathol 1978;90:57–70.
14. Horio T, Nishikimi T, Yoshihara F, et al. Production and secretion of adrenomedullin in cultured rat cardiac myocytes and nonmyocytes: stimulation by interleukin-1 beta and tumor necrosis factor-alpha. Endocrinology 1998;139:4576–80.
15. Thompson NL, Bazoberry F, Speir EH, et al. Transforming growth factor beta-1 in acute myocardial infarction in rats. Growth Factors 1988;1:91–9.
16. Jugdutt BI, Joljart MJ, Khan MI. Rate of collagen deposition during healing and ventricular remodeling after myocardial infarction in rat and dog models. Circulation 1996;94:94–101.
17. Doering CW, Jalil JE, Janicki JS, et al. Collagen network remodelling and diastolic stiffness of the rat left ventricle with pressure overload hypertrophy. Cardiovasc Res 1988;22:686–95.
18. Jugdutt BI. Ventricular remodeling after infarction and the extracellular collagen matrix: when is enough enough? Circulation 2003;108: 1395–403.
19. Rosenkranz AC, Woods RL, Dusting GJ, Ritchie RH. Antihypertrophic actions of the natriuretic peptides in adult rat cardiomyocytes: importance of cyclic GMP. Cardiovasc Res 2003;57:515–22.
20. Pfeffer MA, Braunwald E. Ventricular remodeling after myocardial infarction. Experimental observations and clinical implications. Circulation 1990;81:1161–72.
21. Jugdutt BI. Myocardial salvage by intravenous nitroglycerin in conscious dogs: loss of beneficial effect with marked nitroglycerin-induced hypotension. Circulation 1983;68:673–84.
22. Drummond AH, Beckett P, Brown PD, et al. Preclinical and clinical studies of MMP inhibitors in cancer. Ann NY Acad Sci 1999;878: 228–35.

MOLECULAR AND CELLULAR BIOLOGY, Jan. 2005, p. 136–146 Vol. 25, No. 1
0270-7306/05/$08.00+0 doi:10.1128/MCB.25.1.136–146.2005

Cyclic AMP Potentiates Vascular Endothelial Cadherin-Mediated Cell-Cell Contact To Enhance Endothelial Barrier Function through an Epac-Rap1 Signaling Pathway

Shigetomo Fukuhara,[1] Atsuko Sakurai,[1] Hideto Sano,[2] Akiko Yamagishi,[1] Satoshi Somekawa,[1,3] Nobuyuki Takakura,[2] Yoshihiko Saito,[3] Kenji Kangawa,[4] and Naoki Mochizuki[1]*

Department of Structural Analysis[1] and Department of Biochemistry,[4] National Cardiovascular Center Research Institute, Osaka, Department of Stem Cell Biology, Cancer Research Institute, Kanazawa University, Kanazawa,[2] and First Department of Internal Medicine, Nara Medical University, Nara,[3] Japan

Received 2 August 2004/Returned for modification 2 September 2004/Accepted 28 September 2004

Cyclic AMP (cAMP) is a well-known intracellular signaling molecule improving barrier function in vascular endothelial cells. Here, we delineate a novel cAMP-triggered signal that regulates the barrier function. We found that cAMP-elevating reagents, prostacyclin and forskolin, decreased cell permeability and enhanced vascular endothelial (VE) cadherin-dependent cell adhesion. Although the decreased permeability and the increased VE-cadherin-mediated adhesion by prostacyclin and forskolin were insensitive to a specific inhibitor for cAMP-dependent protein kinase, these effects were mimicked by 8-(4-chlorophenylthio)-2′-*O*-methyladenosine-3′, 5′-cyclic monophosphate, a specific activator for Epac, which is a novel cAMP-dependent guanine nucleotide exchange factor for Rap1. Thus, we investigated the effect of Rap1 on permeability and the VE-cadherin-mediated cell adhesion by expressing either constitutive active Rap1 or Rap1GAPII. Activation of Rap1 resulted in a decrease in permeability and enhancement of VE-cadherin-dependent cell adhesion, whereas inactivation of Rap1 had the counter effect. Furthermore, prostacyclin and forskolin induced cortical actin rearrangement in a Rap1-dependent manner. In conclusion, cAMP-Epac-Rap1 signaling promotes decreased cell permeability by enhancing VE-cadherin-mediated adhesion lined by the rearranged cortical actin.

Endothelial cells lining blood vessels regulate endothelial barrier function, which restricts the passage of plasma proteins and circulating cells across the endothelial cells. Endothelial barrier dysfunction results in an increase in vascular permeability, thereby causing edema or inflammatory or metastatic cell infiltration. Inflammatory mediators such as thrombin and histamine induce intercellular gap formation, leading to an increase in endothelial permeability (1, 4). In contrast, angiopoietin 1 and sphingosine-1-phosphate (S1P) stabilize endothelial barrier integrity (17, 18). In addition, cyclic AMP (cAMP), a second messenger downstream of Gs-coupled receptor, improves endothelial cell barrier function (32, 39, 43). Consistently, cAMP-elevating G protein-coupled receptor (GPCR) agonists, adrenomedullin (AM), prostacyclin (PGI2), prostaglandin E2 (PGE2), and β-adrenergic agonists reduce endothelial hyperpermeability induced by inflammatory stimuli (15, 19, 25).

The endothelial cell barrier is structurally organized by adherens junctions (AJ) and tight junctions. Vascular endothelial (VE) cells express both VE-cadherin (also known as cadherin-5 and CD144) and neural (N)-cadherin (9, 33). VE-cadherin constitutes AJ, whereas N-cadherin formed the cell-cell contacts between endothelial cells and endothelial cell-supporting pericytes. VE-cadherin mediates calcium-dependent, homophilic intercellular adhesion. Its short cytoplasmic tail binds to three armadillo family proteins, β-, γ-, and p120-catenins. β- and γ-catenins associated with α-catenin link the VE-cadherin complex to the actin cytoskeleton and, therefore, strengthen the AJ adhesiveness (9).

Endothelial AJ are dynamic structures, and their adhesive property is finely regulated by several different mechanisms. Tyrosine phosphorylation of VE-cadherin, β-catenin, and p120-catenin correlates with weakened endothelial cell-cell adhesion. VE growth factors and inflammatory mediators such as histamine and thrombin induce tyrosine phosphorylation of AJ components, resulting in the weakened cell-cell contacts and increased endothelial cell permeability (1, 14, 40). In clear contrast, angiopoietin 1, which stabilizes cell-cell contacts, induces dephosphorylation of endothelial cell adhesion molecules, VE-cadherin, and platelet endothelial cell adhesion molecule 1 (17). It has been also reported that S1P induces AJ formation and enhances barrier function through a Rac-dependent cortical actin rearrangement (18). cAMP-dependent protein kinase A (PKA) is suggested to be crucial for cAMP-triggered stabilization of cell-cell contacts and for barrier integrity of endothelial cells (43). However, it has not been clear whether PKA-independent signaling is involved in the regulation of endothelial barrier function.

Rap1, belonging to Ras family GTPase, is involved in the formation and stabilization of AJ in *Drosophila melanogaster* (23). Rap1 becomes the GTP-bound active form by guanine

* Corresponding author. Mailing address: Department of Structural Analysis, National Cardiovascular Center Research Institute, 5-7-1 Fujishirodai, Suita, Osaka 565-8565, Japan. Phone: 81-6-6833-5012, ext. 2508. Fax: 81-6-6835-5461. E-mail: nmochizu@ri.ncvc.go.jp.

nucleotide exchange factor (GEF) and the GDP-bound inactive form by GTPase-activating proteins (GAP), respectively. GEFs for Rap1 include C3G, CalDAG-GEFs, Epacs, and DOCK4 (reviewed in reference 6). DOCK4, which is disrupted in various types of human cancers, regulates the formation of AJ (41). Very recent reports also revealed that Rap1 activity is required for the formation of E-cadherin-based cell-cell contacts (20, 36). These findings prompted us to investigate how Rap1 is activated to stabilize cell-cell contacts and to examine the physiological consequence of stabilized cell-cell contacts by Rap1.

In the present study, we investigated the mechanism by which cAMP-elevating GPCR agonists potentiate endothelial barrier function and restrict cell permeability. We found that increased cAMP triggers Epac-Rap1 signaling to reduce permeability independently of PKA by augmentation of VE-cadherin-mediated cell-cell adhesion.

MATERIALS AND METHODS

Reagents and antibodies. Human recombinant AM was kindly provided by Shionogi & Co. Ltd (31). Materials were purchased as follows: isoproterenol (Iso), PGE2, PGI2, thrombin, forskolin (FSK), and 3-isobutyl-1-methylxanthine (IBMX) from Wako Pure Chemical Industries; dibutyryl-cAMP (dbcAMP) from Sigma-Aldrich; H89 from Seikagaku Corporation; 8-(4-chlorophenylthio)-2′-*O*-methyladenosine-3′,5′-cyclic monophosphate (8-CPT-2′-O-Me-cAMP) from Tocris; fluorescein isothiocyanate (FITC)-labeled dextran (molecular weight, 42,000) and purified human immunoglobulin G (IgG) Fc protein from ICN Biologicals; vascular endothelial growth factor (VEGF) from R & D Systems. Anti-Rap1GAPII antibody was developed by immunization of glutathione *S*-transferase (GST)-tagged Rap1GAPII (amino acids 411 to 694 of Rap1GAPII). Other antibodies used here were purchased as follows: anti-VE-cadherin from Chemicon International and Transduction Laboratories; anti-β-catenin from Transduction Laboratories; anti-CREB and anti-phospho-CREB (Ser133) from Cell Signaling Technology; anti-Rap1 from Santa Cruz Biotechnology; anti-cortactin from Upstate Biotechnology, Inc.; rhodamine-phalloidin and Alexa 488-labeled goat anti-mouse IgG from Molecular Probes; horseradish peroxidase-coupled goat anti-mouse and goat anti-rabbit IgG from Amersham Biosciences.

Cell culture and transfection. Human umbilical vein endothelial cells (HUVECs) and human arterial endothelial cells (HAECs) were purchased from Kurabo (Kurashiki, Japan). The cells were maintained in HuMedia-EG2 with a growth additive set as described previously (12) and used for experiments before passages 7 and 10, respectively. HEK293, 293T, and HeLa cells were maintained in Dulbecco's modified Eagle's medium (DMEM; Nissui, Tokyo, Japan) supplemented with 10% fetal bovine serum and antibiotics (100 μg of streptomycin/ml and 100 U of penicillin/ml). HUVECs and 293T cells were transfected by using Lipofectamine Plus reagent (Invitrogen) and by the calcium-phosphate precipitation technique, respectively.

Plasmids and adenovirus. pcDNA-VE-cad-Ect-Fc-His is a modified vector of pcDNA3.1-Fc-PECAM-1 (a kind gift from W. A. Muller, Cornell University) for producing the secreted form of the extracellular domain of VE-cadherin fused with Fc followed by a six-His tag. A DNA fragment encoding human Epac lacking the cAMP binding domain (amino acids 324 to 881) was amplified by PCR with pMT2SM-HA-Epac (a kind gift from J. L. Bos, Utrecht University, Utrecht, The Netherlands) as a template and ligated into the pCXN2 vector (12). pCXN2-FLAG-Rap1V12-IRES-EGFP expressed both FLAG-tagged Rap1V12 and internal ribosomal entry site (IRES)-driven enhanced green fluorescent protein (EGFP), and pCXN2-Rap1GAPII-IRES-EGFP expressed both FLAG-tagged Rap1GAPII and IRES-driven EGFP. pGL3 control vector was purchased from Promega Corp. Recombinant adenoviruses encoding Rap1GAPII (Ad-RapGAP) and LacZ (Ad-LacZ) were obtained from S. Hattori (The Institute of Medical Science, University of Tokyo) and M. Matsuda (Research Institute for Microbial Disease, Osaka University, Osaka, Japan), respectively. Adenoviruses expressing FLAG-tagged Rap1V12 and IRES-driven EGFP (Ad-Flag-Rap1V12-IRES-EGFP) were produced by using the Adeno-X system according to the manufacturer's protocol (Clontech). Endothelial cells were infected with adenoviruses at the appropriate multiplicities of infection (MOI) as described in the figure legends.

Permeability assay. Permeability across the endothelial cell monolayer was measured by using type I collagen-coated transwell units (6.5-mm diameter, 3.0-μm-pore-size polycarbonate filter; Corning Costar Corporation). HUVECs plated at 10^5 cells in each well were cultured for 3 to 4 days before experiments. After serum starvation in medium 199 containing 1% bovine serum albumin (BSA) for 1 h, the cells were treated with the agonists or drugs, as indicated in the figure legends, for 30 min. Permeability was measured by adding 1 mg of FITC-labeled dextran (molecular weight, 42,000)/ml together with or without 2 U of thrombin/ml to the upper chamber. After incubation for 30 min, 50 μl of sample from the lower compartment was diluted with 300 μl of phosphate-buffered saline (PBS) and measured for fluorescence at 520 nm when excited at 492 nm with a spectrophotometer F-4500 (Hitachi). HUVECs infected with adenovirus for 24 h after becoming confluent and kept for another 24 h in replaced medium were subjected to a cell permeability assay.

Immunocytochemistry. Monolayer-cultured HUVECs grown on a 35-mm-diameter glass base dish (Asahi Techno Glass) were starved in medium 199 containing 0.5% BSA for 3 h and subsequently incubated with the stimulants indicated in the figure legends for 30 min. After stimulation, the cells were fixed in PBS containing 2% formaldehyde for 30 min at 4°C, washed with PBS, and permeabilized with 0.05% Triton X-100 for 30 min at 4°C. Cells were blocked with PBS containing 4% BSA for 1 h at room temperature (RT) and stained with rhodamine-phalloidin for 20 min, anti-VE-cadherin for 60 min, and anticortactin for 60 min at RT. Protein reacting with antibody was visualized with Alexa 488-labeled goat anti-mouse IgG. Images were recorded with a confocal microscope (BX50WI, Fluoview; Olympus) with a water immersion objective lens (LUMPlanF1 100X1.00W).

VE-cadherin translocation assay and Western blot analysis. HUVECs plated in six-well plates were serum starved in medium 199 containing 1% BSA overnight. The cells were stimulated with PGI2 and FSK for the indicated time and fractionated with cytoskeleton-stabilizing buffer (10 mM HEPES [pH 7.4], 250 mM sucrose, 150 mM KCl, 1 mM EGTA, 3 mM $MgCl_2$, 1× protease inhibitor cocktail [Roche Diagnostics], 1 mM Na_3VO_4, 0.5% Triton X-100) by centrifugation at 15,000 × *g* for 15 min. The Triton X-100-insoluble fraction was subjected to sodium dodecyl sulfate-polyacrylamide gel electrophoresis (SDS-PAGE) followed by transfer to Immobilon-P (Amersham Biosciences) and immunoblotting with the indicated antibodies. Immunocomplexes were visualized by enhanced chemiluminescence detection (Amersham Biosciences) with species-matched peroxidase-conjugated secondary antibodies.

Purification of recombinant VE-cadherin ectodomain-Fc chimeric protein. 293T cells transfected with pcDNA-VE-cad-Ect-Fc-His were cultured in DMEM supplemented with 10% fetal calf serum for 24 h and subsequently kept in replaced medium (DMEM-F21 containing 1% fetal calf serum) for 7 days. VE-cadherin-Fc (VEC-Fc) protein secreted into the medium was collected every 2 days and centrifuged to remove floating cells and debris. VEC-Fc was collected on ProBond resin (Invitrogen) by gentle agitation overnight at 4°C. VEC-Fc protein bound to the beads was eluted with 500 mM imidazole, concentrated with Amicon Centriplus 30 (Millipore), and buffer exchanged into PBS containing 2 mM $CaCl_2$ and 2 mM $MgCl_2$ (PBS-Ca/Mg) by dialysis.

Cell adhesion assay. Twenty-four-well tissue culture plates were coated with 10 μg of VEC-Fc or Fc protein/ml in PBS-Ca/Mg at 4°C overnight. After washing with PBS-Ca/Mg, the plates were blocked with 1% heat-inactivated BSA in PBS (heat inactivated at 85°C for 12 min) for 1 h at RT. To examine cell adhesion to the VEC-Fc- or Fc-coated dish, cells were suspended in 0.5% BSA-containing medium 199 and incubated for 30 min at 37°C. Cells (1.5×10^5) were plated on each VEC-Fc- or Fc-coated well in the presence or absence of agonists, drugs, and 5 mM EGTA and adhered to the dish at 37°C for the indicated time. To analyze cell adhesion to a collagen-covered surface, cells were plated onto a collagen-coated six-well plate (Iwaki) and adhered to the dish in the presence or absence of 5 mM EGTA. After washing with PBS-Ca/Mg four times to remove nonadherent cells, adherent cells and input cells were quantified by measuring endogenous alkaline phosphatase activity as described elsewhere (35). Briefly, the cells were lysed in a buffer containing 100 mM Tris-citrate (pH 6.5) and 0.25% Triton X-100, and alkaline phosphate activity in the lysate was measured by using the AttoPhos AP fluorescent substrate system (Promega Corp.). To examine the effects of Rap1V12, EpacΔcAMP, and Rap1GAPII, HUVECs were transfected with plasmids encoding either Rap1V12, EpacΔcAMP, or Rap1GAPII together with the luciferase reporter construct (pGL3 control vector). The adhesion of cells expressing Rap1V12, EpacΔcAMP, or Rap1GAPII to the VEC-Fc-coated dish was normalized by measuring the luciferase activity of the cells and input cells (16).

Detection of GTP-bound form of Rap1. Rap1 activity was assessed by a modified Bos's method as described previously (34). Briefly, HUVECs starved in medium 199 containing 1% BSA overnight were stimulated with the indicated

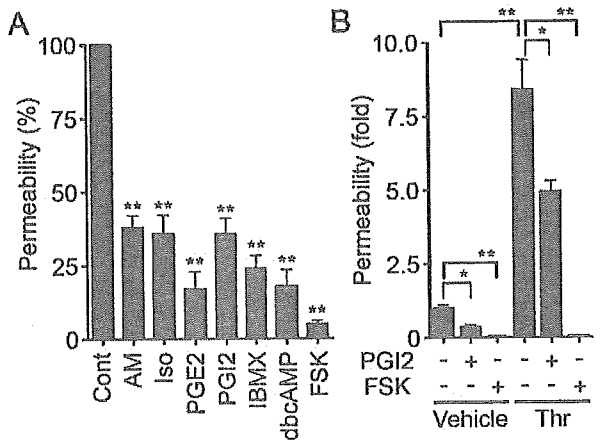

FIG. 1. cAMP enhances barrier function of monolayer VE cells. (A) Vascular permeability, reflecting barrier function, was analyzed by measuring the fluorescence of FITC-labeled dextran across the monolayer-cultured HUVECs as described in Materials and Methods. HUVECs grown on transwell filters were incubated with control (Cont), 0.1 μM AM, 200 μM Iso, 200-ng/ml PGE2, 10-μg/ml PGI2, 1 mM IBMX, 1 mM dbcAMP, and 10 μM FSK for 30 min. Average permeability ± standard deviation is expressed as a percentage compared to the control. (B) The effects of PGI2 and FSK on vascular permeability were quantified in the presence (+) or absence (−) (Vehicle) of 2 U of thrombin (Thr)/ml. Average permeability ± standard deviation is expressed as the increase relative to that observed in unstimulated HUVECs in the vehicle. Data shown are the results from at least three independent experiments. Significant differences from the control (A) or between two groups (B) determined by Student's *t* test are indicated by a single asterisk ($P < 0.05$) or double asterisks ($P < 0.01$).

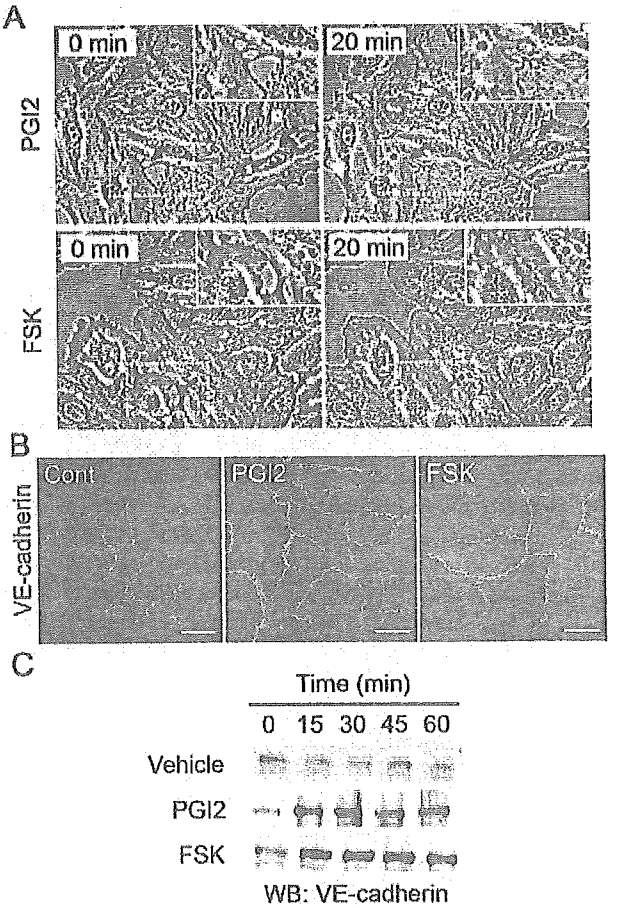

FIG. 2. cAMP induces AJ formation. (A) HUVECs cultured on a glass base dish were stimulated with 10 μg of PGI2/ml (upper panels) or with 10 μM FSK (lower panels) for 20 min and shown as phase-contrast images. Left and right panels show the cells before and after stimulation, respectively. The arrows indicate the sites of cell-cell contacts induced by PGI2 and FSK. The area boxed by the white broken line is enlarged in the right top of the panels. Bars, 50 μm. (B) Subconfluent HUVECs stimulated with vehicle (Cont), 10-μg/ml PGI2, and 10 μM FSK for 45 min were fixed, stained with anti-VE-cadherin antibody, and visualized with Alexa 488-conjugated secondary antibody through a confocal microscope (BX50WI; Olympus). Note that VE-cadherin (green) was accumulated at the cell-cell contact upon PGI2 and FSK stimulation. Bars, 50 μm. (C) Translocation of VE-cadherin was assessed by Triton X-100 solubility. HUVECs were stimulated with vehicle (top), 10-μg/ml PGI2 (middle), and 10 μM FSK (bottom) for the time indicated at the top and fractionated with cytoskeleton-stabilizing buffer as described in Materials and Methods. The Triton X-100-insoluble fraction was subjected to SDS-PAGE followed by Western blot analysis (WB) with anti-VE-cadherin.

agonists and drugs and lysed at 4°C in a pull-down lysis buffer (20 mM Tris-HCl [pH 7.5], 100 mM NaCl, 10 mM $MgCl_2$, 1% Triton X-100, 1 mM EGTA, 1 mM dithiothreitol, 1 mM Na_3VO_4, 1× protease inhibitor cocktail). GTP-bound Rap1 was collected on the GST-Rap1 binding domain of RalGDS precoupled to glutathione-Sepharose beads and subjected to SDS-PAGE followed by immunoblotting with anti-Rap1.

In vivo permeability assay. In vivo permeability was quantified by a modified Miles assay as described previously (29). In brief, ICR mice (Japan SLC, Inc.) shaved 3 days before experiments were lightly anesthetized and intravenously injected with 150 μl of 1% Evans blue dye solution (in saline) passed through a 0.22-μm-pore-size filter. Fifteen minutes later, 20 μl of PBS, VEGF (50 μg/ml), and/or 8-CPT-2′-O-Me-cAMP (1 mM) were applied by intradermal injections with a 30-gauge needle. The sites of intradermal injection were photographed 60 min after the injection, carefully dissected, and weighed. To quantify the vascular permeability, extravasated blue dye was eluted from the dissected skin with formamide at 56°C, and optical density was measured by spectrophotometry at 620 nm.

RESULTS

cAMP enhances the barrier property of monolayer-cultured endothelial cell. To evaluate the barrier function, we examined the permeability of FITC-labeled dextran across monolayer HUVECs. Expectedly, AM, Iso, PGE2, and PGI2 reduced basal endothelial permeability in HUVECs (Fig. 1A). PGI2 also reduced thrombin-induced vascular permeability (Fig. 1B). Other cAMP-elevating bio-ligands similarly reduced thrombin-induced permeability (data not shown). The bio-ligands for cAMP-elevating GPCR that we used in this study indeed increased cAMP in HUVECs (data not shown). Furthermore, IBMX (an inhibitor for phosphodiesterase), dbcAMP (a membrane-permeable cAMP analogue), and FSK (an adenylyl cyclase activator) resulted in a reduction of both basal and thrombin-induced endothelial permeability (Fig. 1; data not shown).

cAMP potentiates formation of AJ. Endothelial barrier function is largely dependent upon endothelial cell junctions. To investigate how cAMP affects AJ formation, we examined AJ organization by immunostaining with anti-VE-cadherin before and after stimulation. When subconfluent HUVECs with intercellular gaps were stimulated with PGI2 or FSK, the cells extended the plasma membrane and established cell-cell contacts with neighboring cells (Fig. 2A). Similar results were

obtained with AM and PGE2 (data not shown). Stimulation of HUVECs with PGI2 and FSK dramatically enhanced accumulation of VE-cadherin at cell-cell contacts (Fig. 2B).

The maturation of AJ requires homophilic binding of intercellular VE-cadherins and tight anchoring to the actin cytoskeleton via the cytoplasmic region through catenins. VE-cadherin anchored to the actin cytoskeleton is detected in detergent-insoluble fractions of cell lysates (26). We found an increase in VE-cadherin in the Triton X-100-insoluble fraction after stimulation with PGI2 or FSK (Fig. 2C). These results suggest that cAMP-elevating GPCR agonists potentiate AJ formation, which results in a cAMP-induced decrease in permeability.

cAMP promotes VE-cadherin-dependent endothelial cell adhesion. VE-cadherin is required for AJ formation (9). To test the involvement of a homophilic interaction of VE-cadherin in cAMP-enhanced AJ formation, we directly examined VE-cadherin-mediated cell adhesion. To mimic the VE-cadherin-dependent cell adhesion, we used VEC-Fc chimeric protein, which consisted of the extracellular domain of VE-cadherin fused to the Fc portion of immunoglobulin. HUVECs were plated onto VEC-Fc-coated dishes and time-lapse imaged. Cells attached within 5 min to the VEC-Fc-coated dish, subsequently spread, and exhibited a typical fried-egg morphology characterized by a large circular lamellipodium (Fig. 3A). No cells attached to the Fc-coated dish (Fig. 3B and C). Since cadherin-dependent cell adhesion requires Ca^{2+}, we examined the effect of Ca^{2+} chelation on cell adhesion to VEC-Fc-coated dishes. Cell adhesion to VEC-Fc-coated dishes was completely abolished by chelating extracellular Ca^{2+}, although cell attachment to the collagen-coated dish was unaffected (Fig. 3C and D). Basal and FSK-augmented cell adhesion to VEC-Fc-coated dishes was inhibited by EGTA (Fig. 3C). Both HUVECs and HAECs expressing VE-cadherin adhered to the VEC-Fc-coated dish (Fig. 3E). In clear contrast, HeLa and HEK293 cells, which express N-cadherin, but not VE-cadherin (20, 42), did not adhere to the VEC-Fc-coated dish, although these cells could attach to the collagen-coated dish (Fig. 3E; data not shown). Collectively, these results indicate that endothelial cell adhesion to the VEC-Fc-coated dish depends upon the homophilic ligation of VE-cadherin.

We proceeded to investigate the effect of cAMP-elevating GPCR agonists on VE-cadherin-mediated cell adhesion. The adhesion of HUVECs plated in the presence of PGI2 or FSK was evaluated by the alkaline phosphatase activity of remaining cells after washing. PGI2 enhanced adhesion of HUVECs to the VEC-Fc-coated dish in a concentration-dependent manner (Fig. 4A) and in a time-dependent manner (Fig. 4B). In a time course analysis, we noticed that enhanced adhesion was observed 7 min after the plating (Fig. 4B). Other cAMP-elevating GPCR agonists, including AM, Iso, and PGE2, potentiated VE-cadherin-dependent cell adhesion (Fig. 4C). In addition, similarly enhanced cell adhesion to the VEC-Fc-coated dish was also observed in the cells treated with cAMP-elevating drugs such as IBMX, dbcAMP, and FSK (Fig. 4F). Like PGI2, the effect of FSK on cell adhesion to the VEC-Fc-coated dish was concentration dependent and time dependent (Fig. 4D and E). This cAMP-induced cell adhesion to the VEC-Fc-coated dish depends on the enhanced homophilic ligation of VE-cadherin because FSK did not augment endothelial adhe-

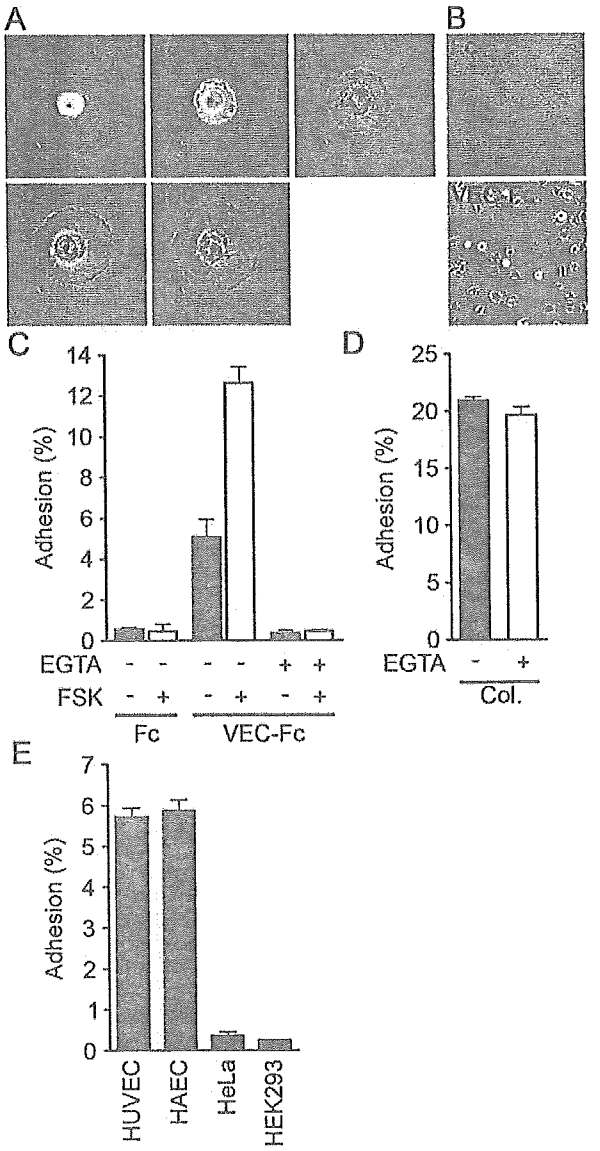

FIG. 3. Endothelial cells adhere to a VEC-Fc-coated dish through homophilic ligation of VE-cadherin. (A) HUVECs were plated onto the VEC-Fc-coated dish and time-lapse imaged at the time points (in minutes) indicated on the panels. Bar, 20 μM. (B) HUVECs were plated on the Fc-coated dish (top panel) or the VEC-Fc-coated dish (bottom panel) for 1 h and phase-contrast imaged after removal of nonadherent cells by washing with PBS-Ca/Mg. (C) HUVECs were plated onto either an Fc- or VEC-Fc-coated dish in the absence (−) or presence (+) of 5 mM EGTA and 10 μM FSK for 7 min. Cell adhesion was quantified as described in Materials and Methods. (D) Adhesion of HUVECs to a collagen-coated dish in the presence or absence of 5 mM EGTA was analyzed by a method similar to that described for panel C. (E) Adhesion of HUVECs, HAECs, and HeLa and HEK293 cells to the VEC-Fc-coated dish was examined as described in the legend for panel C. Cells adhering to the dishes of total input cells (percentage) is expressed as the mean ± standard deviation by measuring alkaline phosphatase activity of adherent cells divided by that of total input cells. Representative results from three independent experiments were shown in all panels.

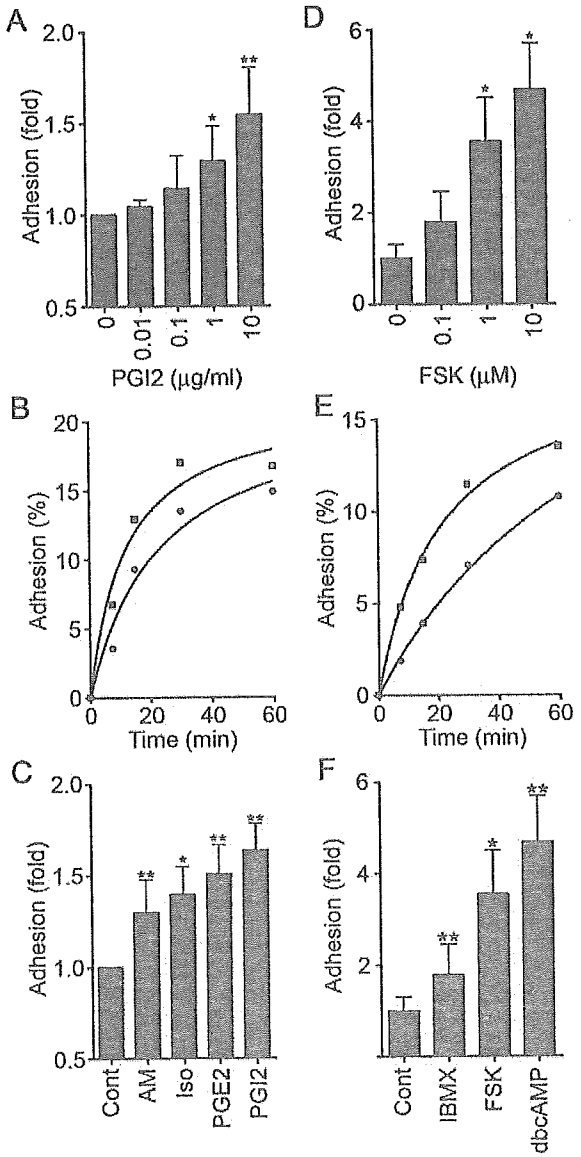

FIG. 4. cAMP potentiates VE-cadherin-dependent cell adhesion. (A) HUVECs were plated onto a VEC-Fc-coated dish in the presence of PGI2 at the concentrations indicated at the bottom for 7 min. Cell adhesion was quantified as described in Materials and Methods. Mean adhesion activity ± standard deviation is expressed as the increase compared with that observed in unstimulated cells. (B) HUVECs were plated onto the VEC-Fc-coated dish in the absence (circle) or presence (square) of 10-μg/ml PGI2 for the time indicated at the bottom. The percent adhesion was calculated by measuring the alkaline phosphatase activity of adherent cells divided by that of total input cells. (C) HUVECs stimulated with cAMP-elevating ligands similar to that described in the legend to panel A were assessed for adhesion activity. The concentration of stimulants was the same as described in the legend to Fig. 1A. (D) The effect of FSK on cell adhesion was analyzed by a method similar to that described for panel A, except that cells were preincubated for 10 min before plating. (E) The effect of 10 μM FSK on time-dependent adhesion was analyzed as described in the legend to panel B, except that cells were preincubated for 10 min before plating. (F) HUVECs stimulated with the reagent indicated at the same concentration used as described in the legend to Fig. 1A were analyzed for cell adhesion by a method similar to that described for panel D. Data are expressed as means ± standard deviations of the results from three independent experiments in panels A, C, D, and F. Representative results from three independent experiments were shown in panels B and E. A significant difference from the control determined by Student's t test is indicated with a single asterisk ($P < 0.05$) or double asterisks ($P < 0.01$).

sion to the Fc-coated dish or attachment to the VEC-Fc-coated dish in the absence of extracellular Ca^{2+} (Fig. 3C). These results indicate that cAMP potentiates VE-cadherin-dependent cell adhesion.

cAMP augments endothelial barrier function in a PKA-independent manner. PKA is suggested to be involved in cAMP-enhanced endothelial barrier function (43). Thus, we investigated the involvement of PKA in the regulation of endothelial barrier integrity by PGI2 and FSK. Unexpectedly, PGI2- and FSK-induced reduction of endothelial permeability was insensitive to a specific PKA inhibitor, H89 (7) (Fig. 5A and B). The reduction of thrombin-increased permeability by FSK was also unaffected by H89 (Fig. 5C). Consistently, H89 did not affect VE-cadherin-mediated cell adhesion enhancement by PGI2 and FSK (Fig. 5D and E). To confirm that H89 worked in HUVECs, we examined FSK-induced phosphorylation of CREB, a direct PKA substrate (38). Phosphorylation of CREB upon FSK stimulation was significantly inhibited by H89, indicating the effectiveness of this inhibitor in HUVECs (Fig. 5F). Therefore, these results apparently suggest a novel PKA-independent signaling pathway involved in cAMP-induced endothelial barrier function.

cAMP induces Rap1 activation. Besides PKA, Epac (cAMP-GEF) was identified as a novel cAMP target and a Rap1-specific GEF (5, 21). We therefore hypothesized that cAMP-activated Epac-Rap1 signaling is involved in the enhancement of VE-cadherin-dependent cell adhesion and endothelial barrier function. To address this possibility, we tested whether cAMP-elevating GPCR agonists induce Rap1 activation in HUVECs. Rap1 activity was determined by a pull-down assay by using a GST fusion protein of Rap1-binding domain of RalGDS according to the Bos's method. Bio-ligands for cAMP-elevating GPCR activated Rap1 (Fig. 6A). PGI2 rapidly induced Rap1 activation, which peaked at 1 to 5 min after the stimulation and then declined to the basal level by 10 min (Fig. 6C). A second wave of Rap1 activation was also observed 15 to 45 min after the stimulation (Fig. 6C). PGI2-induced Rap1 activation occurred in a concentration-dependent manner (Fig. 6B), which was associated with enhancement of VE-cadherin-dependent cell adhesion (Fig. 4A). Similarly, dbcAMP, FSK, and IBMX activated Rap1 (Fig. 6D). FSK-induced Rap1 activation reached a maximal level 2 to 5 min after the stimulation, and the level was sustained for up to 15 to 30 min (Fig. 6E). Collectively, these findings indicate that cAMP induces Rap1 activation in endothelial cells.

Specific activation of Epac reduces endothelial permeability and enhances VE-cadherin-dependent cell adhesion. To test whether the activation of endogenous Epac is sufficient to reduce endothelial permeability and to induce VE-cadherin-dependent cell adhesion, we used a recently developed cAMP analog, 8-CPT-2′-O-Me-cAMP, which specifically activates Epac without affecting PKA activity (13). As expected, 8-CPT-2′-O-Me-cAMP induced Rap1 activation in HUVECs (Fig. 7A), indicating that Epac is expressed in endothelial cells.

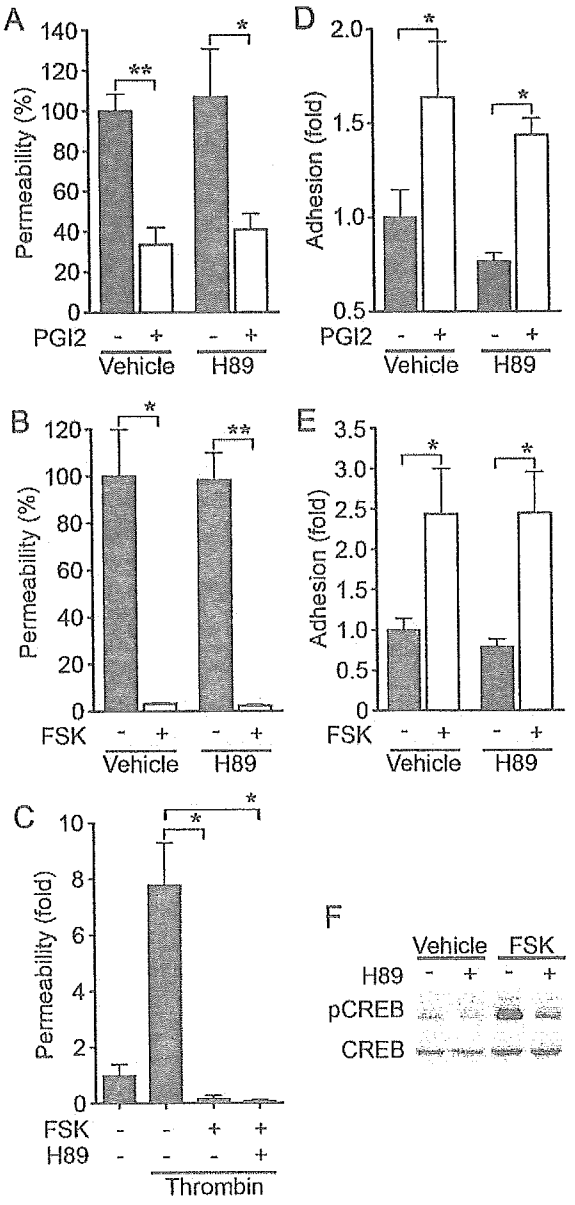

FIG. 5. cAMP-enhanced VE-cadherin-dependent cell adhesion and endothelial barrier function does not depend upon PKA. (A) Permeability across monolayer HUVECs grown on transwell filters were assessed by measuring FITC-labeled dextran as described in the legend to Fig. 1A. The effect of 10-μg/ml PGI2 on cell permeability without pretreatment (Vehicle) or with pretreatment with 5 μM H89, a specific PKA inhibitor, for 10 min is indicated as the percent permeability compared to that observed in untreated cells. +, present; −, absent. (B) The effect of 10 μM FSK on cell permeability without pretreatment (Vehicle) and with pretreatment with H89 was assessed similar to that described for panel A. (C) The effect of pretreatment of HUVECs with 5 μM H89 on FSK-induced reduction of 2-U/ml thrombin-induced permeability was analyzed. Permeability indicates the increase relative to that observed in untreated cells. (D) HUVECs untreated or pretreated with H89 for 10 min prior to stimulation with 10-μg/ml PGI2 were analyzed for cell adhesion as described in the legend to Fig. 4A. (E) HUVECs untreated or pretreated with H89 for 10 min prior to stimulation with 10 μM FSK were analyzed for cell adhesion as described in the legend to Fig. 4D. For panels A to E, data are expressed as means ± standard deviations of the results from triplicate samples. Similar results were obtained in at least three independent experiments. Significant differences between two groups determined by Student's t test are indicated by a single asterisk ($P < 0.05$) or double asterisks ($P < 0.01$). (F) HUVECs serum starved in 1% BSA-containing medium 199 for 6 h, followed by pretreatment with (+) or without (−) 5 μM H89 for 10 min, were stimulated with vehicle and 10 μM FSK for 10 min. Phosphorylation of CREB was assessed by Western blot analysis with anti-CREB (CREB) and anti-phospho-CREB-specific (pCREB) antibodies.

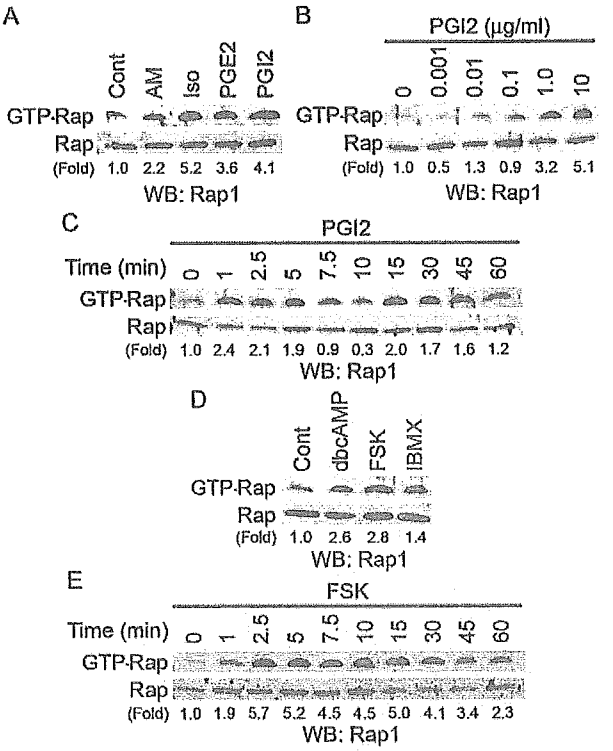

FIG. 6. cAMP induces Rap1 activation. (A) Serum-starved HUVECs kept in medium 199 containing 1% BSA overnight were stimulated with cAMP-elevating agonists for 2.5 min as indicated at the top and at the concentrations described in the legend to Fig. 1A. GTP-bound Rap1 was detected by pull-down assay as described in Materials and Methods. Activation indicates the ratio of the poststimulation GTP-Rap1 intensity of total Rap1 intensity to the prestimulation GTP-Rap1 intensity of total Rap1 intensity. (B) Rap1 activation was analyzed by detecting GTP-bound Rap1 with lysates from HUVECs stimulated with PGI2 for 2.5 min at the different concentrations indicated at the top. (C) Rap1 activation was analyzed by detecting GTP-bound Rap1 with lysates from cells stimulated with 10-μg/ml PGI2 for the time period indicated at the top. (D) Serum-starved HUVECs similar to those described in the legend to panel A were stimulated with the reagents indicated at the top for 10 min at the same concentrations described in the legend to Fig. 1A. Rap1 activation was assessed by a method similar to that described for panel A. (E) The effect of 10 μM FSK on time-dependent Rap1 activity was examined as described for panel C. Representative results from at least three independent experiments are shown for all panels.

8-CPT-2′-O-Me-cAMP dramatically reduced basal endothelial permeability, as did FSK and dbcAMP (Fig. 7B). Thrombin-induced permeability was also inhibited by 8-CPT-2′-O-Me-cAMP (Fig. 7C). Furthermore, we examined the effect of 8-CPT-2′-Me-cAMP on in vivo vascular permeability. VEGF-induced vascular permeability was completely blocked by coinjection of 8-CPT-2′-O-Me-cAMP (Fig. 7D). In addition, adhesion

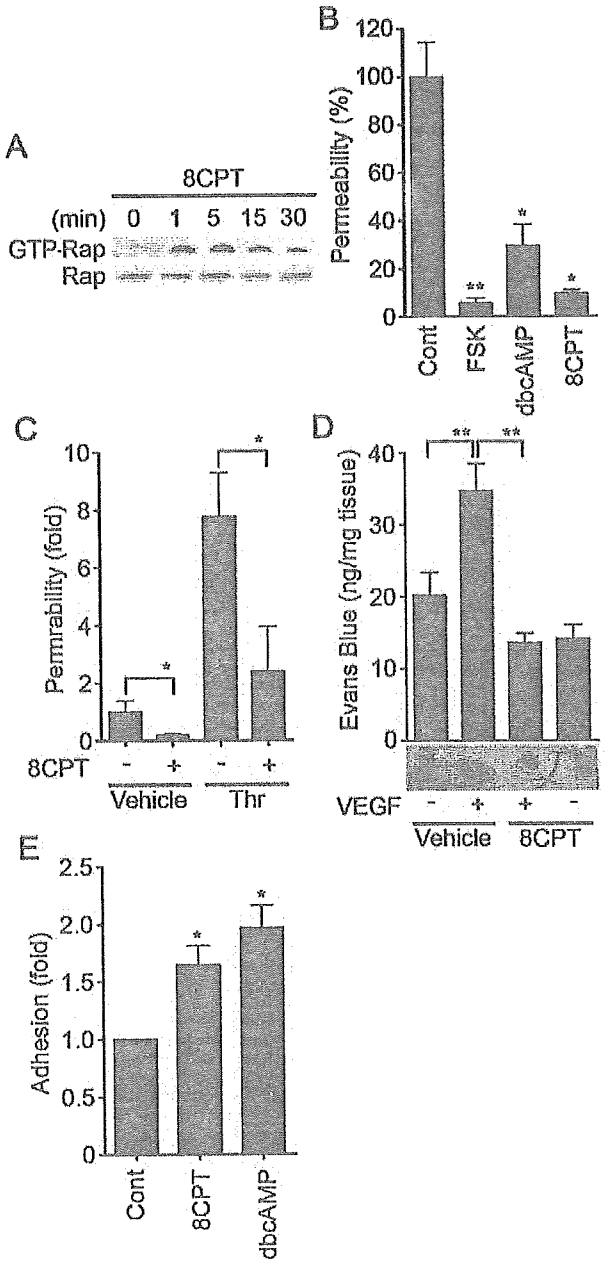

FIG. 7. Activation of Epac is sufficient to enhance VE-cadherin-dependent cell adhesion and endothelial barrier function. (A) Serum-starved HUVECs in medium 199 containing 1% BSA were stimulated with 0.2 mM 8-CPT-2′-O-Me-cAMP (8CPT) for the indicated time. Rap1 activity was determined as described in the legend to Fig. 6A. The result is a representative from three independent experiments. (B) Permeability of cells treated with the reagents as indicated on the bottom for 30 min was analyzed as described in the legend to Fig. 1A. (C) The effect of 0.2 mM 8CPT-2′-O-Me-cAMP on 2-U/ml thrombin-induced permeability was analyzed as described in the legend to Fig. 1B. (D) Effect of 8CPT-2′-O-Me-cAMP on VEGF-induced permeability was assessed by intradermal Miles assay as described in Materials and Methods. Amounts of extravasation of Evan blue in mouse dermal skin were measured 60 min after intradermal injection of vehicle and VEGF together with (+) or without (−) 8CPT. Mean leakage ± standard deviation of the results from 6 mice per group is expressed as nanograms of weight of extravasated Evans blue per milligram of weight of dermal skin. A photograph on the bottom shows leakage of Evans blue in dermal skin. (E) HUVEC adhesion to the VEC-Fc-coated dish in the presence of 0.2 mM 8CPT and 1 mM dbcAMP for 7 min was analyzed as described in the legend to Fig. 4F. In panels B, C, and E, data are expressed as means ± standard deviations of the results from triplicate samples. A significant difference from the control in panels B and E or between two groups in panels C and D was determined by Student's t test and indicated by a single asterisk ($P < 0.05$) or double asterisks ($P < 0.01$).

of HUVECs to the VEC-Fc-coated dish was significantly enhanced by 8-CPT-2′-O-Me-cAMP (Fig. 7E). Hence, Epac activation is sufficient to enhance VE-cadherin-dependent cell adhesion and to augment endothelial barrier function in vitro and in vivo.

Rap1 activation is essential for VE-cadherin-dependent cell adhesion and endothelial barrier function. We next proceeded to investigate the role of Rap1 in VE-cadherin-dependent cell adhesion and endothelial barrier function. To examine the effect of Rap1 on cell permeability and VE-cadherin-mediated cell adhesion, we inactivated endogenous Rap1 by adenovirus-expressing Rap1GAPII (Ad-RapGAP), which specifically catalyzes the hydrolysis of GTP to GDP on Rap1 (30). As shown in Fig. 8A, endogenous Rap1 activity was almost completely suppressed by the expression of increasing amounts of Rap1GAPII in HUVECs. This Rap1 inactivation paralleled the increase in basal permeability (Fig. 8B) and the inhibition of cell adhesion to the VEC-Fc-coated dish (Fig. 8D). In contrast, a constitutively active Rap1, Rap1V12, reduced both basal and thrombin-increased cell permeability (Fig. 8C). VE-cadherin-mediated cell adhesion was also enhanced by Rap1V12 and EpacΔcAMP, a constitutively active mutant of Epac (Fig. 8D). Taken together, these results indicate that Rap1 activation is required for VE-cadherin-mediated cell adhesion and endothelial barrier function.

cAMP enhances VE-cadherin-dependent cell adhesion and endothelial barrier function by activating Rap1. To test the requirement for Rap1 in endothelial barrier enhancement by cAMP-elevating GPCR agonists, we infected HUVECs with Ad-RapGAP and examined the effect of inactivation of Rap1 on PGI2- and FSK-induced reduction of cell permeability. Although basal endothelial permeability was reduced by PGI2 and FSK (Fig. 9A and B), overexpression of Rap1GAPII increased not only basal but also PGI2- and FSK-reduced endothelial permeability, indicating the requirement of Rap1 activity for PGI2- and FSK-induced barrier enhancement. We also investigated the involvement of Rap1 in PGI2- and FSK-induced VE-cadherin-dependent cell adhesion. PGI2 and FSK augmented VE-cadherin-dependent cell adhesion of HUVECs infected with control adenovirus (Ad-LacZ); however, their effects were dramatically suppressed by overexpression of Rap1GAPII (Fig. 9C and D). These data demonstrate that cAMP enhances VE-cadherin-dependent cell adhesion and endothelial barrier functions by activating Rap1.

cAMP induces endothelial cortical actin rearrangement in a Rap1-dependent manner. Endothelial barrier function is largely dependent upon the actin cytoskeleton supporting junctional adhesion molecules (10). Thus, we examined the effect of cAMP on cortical actin polymerization and assembly of polymerized actin in a monolayer of endothelial cells. Cortactin, an actin-binding protein, is known to be implicated in cortical actin rearrangement (8) and suggested to regulate S1P-induced endothelial barrier enhancement (11). PGI2,

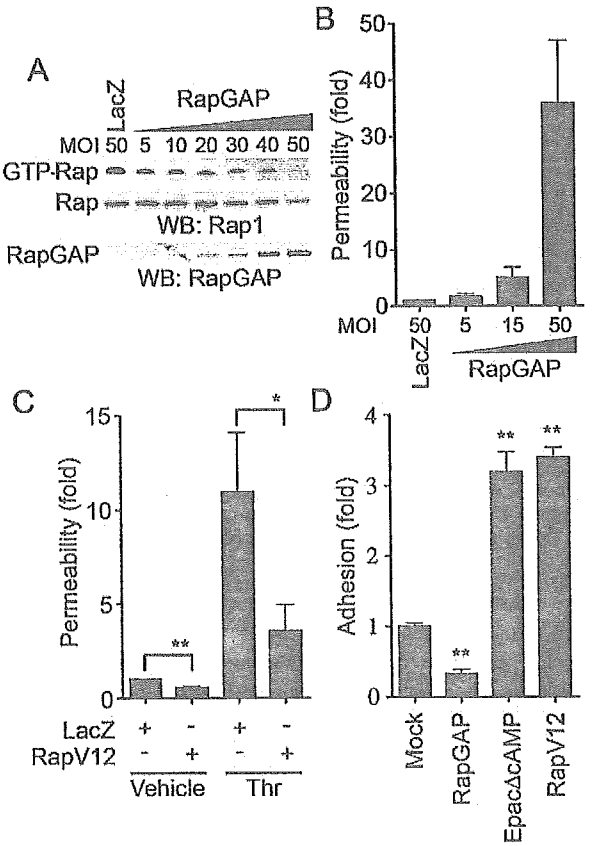

FIG. 8. Rap1 plays a critical role in VE-cadherin-dependent cell adhesion and endothelial barrier function. (A) Rap1 inactivation was assessed by detecting GTP-Rap1 in HUVECs infected with different MOI of adenovirus-expressing Rap1GAPII (RapGAP) as indicated at the top. An adenovirus-expressing LacZ at an MOI of 50 was used as a control. GTP-bound Rap1 (GTP-Rap) was detected by pull-down assay as described in Materials and Methods. Rap1 (Rap) and Rap1GAPII (RapGAP) expression were examined by Western blot analysis. (B) The permeability of FITC-dextran across HUVECs infected with adenovirus as indicated at the bottom was analyzed as described in Materials and Methods. Data are the means ± standard deviations of the results from three independent experiments and are expressed as increases relative to those of LacZ-infected cells. (C) Monolayer HUVECs infected with either an adenovirus-expressing LacZ or that expressing Rap1V12 at an MOI of 50 for 24 h were medium changed and cultured for another 24 h. The permeability of cells upon 2-U/ml thrombin stimulation (Thr) after starvation for 1 h was analyzed as described in the legend to Fig. 1B. Data are the means ± standard deviations of the results from five independent experiments and are expressed as inductions relative to those of untreated HUVECs infected with the LacZ-expressing virus. (D) HUVECs were transfected with either empty vector (Mock), plasmids expressing Rap1GAPII (RapGAP), EpacΔcAMP, or Rap1V12 together with the luciferase reporter construct. Transfected cells were plated on the VEC-Fc-coated dish and allowed to adhere for 15 min. Cell adhesion was analyzed as described in Materials and Methods. Data are expressed as increases compared to those of mock-transfected cells. The results indicate the means ± standard deviations of the results from triplicate samples. Similar results were obtained in three independent experiments. Significant differences between two groups in panel C or from the control in panel D are determined by Student's *t* test and are indicated by a single asterisk ($P < 0.05$) or double asterisks ($P < 0.01$).

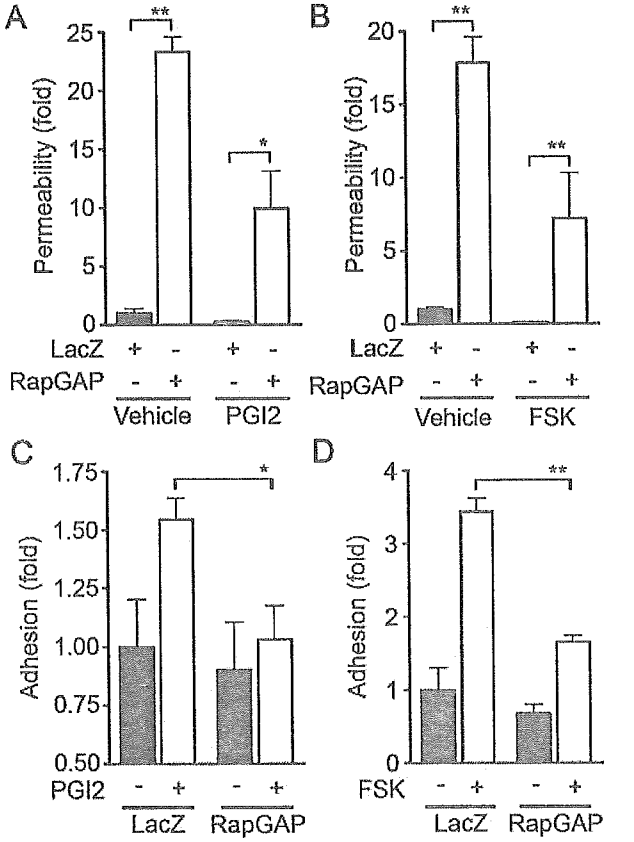

FIG. 9. Inactivation of Rap1 reduces PGI2- and FSK-induced barrier function and VE-cadherin-mediated cell adhesion. (A) Monolayer-cultured HUVECs grown on transwell filters were infected with either LacZ-expressing adenovirus (Ad-LacZ) or Rap1GAPII-expressing virus (Ad-RapGAP) at an MOI of 40 for 24 h. Medium was replaced with fresh medium after infection. Cells were cultured for an additional 24 h and treated with 10 μg of PGI2/ml for 30 min after serum starvation for 1 h. Permeability was analyzed as described in Materials and Methods. (B) The effect of 10 μM FSK on permeability in HUVECs infected with Ad-RapGAP was similarly analyzed. (C) HUVECs were infected with either Ad-LacZ or Ad-RapGAP at an MOI of 40 for 24 h. HUVECs resuspended in medium 199 with 0.5% BSA were plated onto VEC-Fc-coated dishes in the presence (+) or absence (−) of 10 μg of PGI2/ml for 7 min. Cell adhesion activity was quantified as described in the legend to Fig. 4A. (D) The effect of FSK on adhesion of HUVECs infected with Ad-RapGAP was analyzed similarly to that described for panel C. Resuspended HUVECs were preincubated with 10 μM FSK for 10 min before plating. Significant differences between two groups determined by Student's *t* test are indicated by a single asterisk ($P < 0.05$) or double asterisks ($P < 0.01$).

FSK, and 8-CPT-2′-O-Me-cAMP dramatically induced accumulation of polymerized actin and cortactin at cell-cell contacts (Fig. 10A). To explore the involvement of Rap1 in cAMP-mediated cortical actin rearrangement, an expression vector encoding Rap1GAPII was introduced into endothelial cells. FSK enhanced actin polymerization at cell-cell contacts in cells transfected with control vector encoding EGFP, whereas it did not in cells expressing Rap1GAPII (Fig. 10B). Cytochalasin D, an actin-depolymerizing agent, attenuated FSK-induced barrier enhancement (Fig. 10C) and inhibited FSK-induced VE-cadherin-dependent cell adhesion (Fig. 10D). These results suggest that the cortical actin rearrangement promoted by

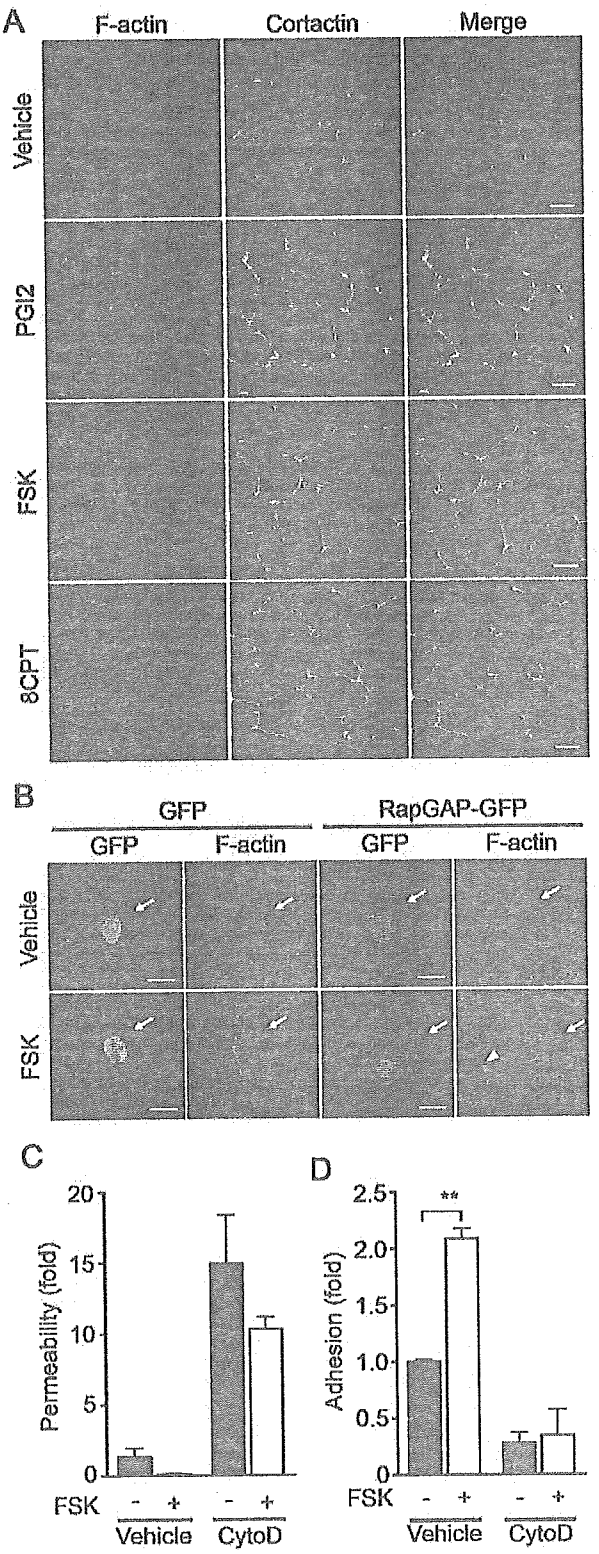

FIG. 10. cAMP induces cortical actin rearrangement in a Rap1-dependent manner. (A) Monolayer-cultured HUVECs starved in 0.5% BSA-containing medium 199 for 3 h were stimulated with vehicle (top row), 10-μg/ml PGI2 (second row), 10 μM FSK (third row), and 0.2 mM 8-CPT-2′-O-Me-cAMP (8CPT) (bottom row) for 30 min. Fixed and permeabilized cells were stained with rhodamine-phalloidin (left column) and with anti-cortactin (center column). Rhodamine images to detect F-actin (red) and Alexa 488 images for cortactin visualized by Alexa 488-labeled secondary antibody (green) were obtained through a confocal microscope (BX50WI). Right panels show the merged images of rhodamine and Alexa 488 images. Bars, 20 μm. (B) HUVECs transfected with an EGFP-expressing vector (left) and pCXN2-Rap1GAPII-IRES-EGFP (right) were serum starved in 0.5% BSA-containing medium 199 for 3 h and stimulated with vehicle (top panels) and 10 μM FSK (bottom panels). Cells were fixed, permeabilized, and stained with Rhodamine-phalloidin. EGFP images (green) and rhodamine images showing F-actin (red) were obtained similar to those in panel A. Arrows and arrowhead indicate transfected and untransfected cells, respectively. Bars, 20 μm. (C) Cell permeability of HUVECs pretreated with 2 μM cytochalasin D (CytoD) for 30 min followed by 10 μM FSK stimulation for 30 min was analyzed as described in the legend to Fig. 1A. −, absent; +, present. (D) The effect of pretreatment of 2 μM cytochalasin D (CytoD) on adhesion of HUVECs stimulated with FSK was analyzed as described in the legend to Fig. 5E. A significant difference between two groups determined by Student's t test is indicated by double asterisks ($P < 0.01$).

cAMP-Epac-Rap1 signaling may contribute to the potentiation of endothelial barrier function and VE-cadherin-dependent cell adhesion.

DISCUSSION

cAMP is a well-known intracellular signaling molecule that is capable of restoring diminished endothelial barrier function. Previous reports suggested that cAMP-induced barrier enhancement occurs through PKA (27, 39). In this study, however, we demonstrated a novel PKA-independent signaling pathway, the cAMP-Epac-Rap1 signaling pathway, involved in cAMP-induced barrier function based on the following observations. PGI2- and FSK-reduced endothelial permeability was insensitive to H89. A specific activator for Epac, 8-CPT-2′-O-Me-cAMP, reduced both basal and thrombin-increased permeability. Plasma leakage in response to VEGF was also inhibited by 8-CPT-2′-O-Me-cAMP in vivo. We found that the activation of Rap1 leads to decreased permeability. Not only all cAMP-elevating bio-ligands we tested but also FSK, db-cAMP, and IBMX activated Rap1. Consistently, cAMP-dependent Rap1 activation upon stimulation by these ligands involved Epac in the regulation of barrier function. A previous report showed that Rap1 is phosphorylated by PKA in neutrophils and platelets, although the function of phosphorylated Rap1 has not been elucidated (37). So far, Epac is known to regulate several biological functions including integrin-dependent cell adhesion, insulin secretion, and calcium release through ryanodine-sensitive Ca^{2+} channels (reviewed in reference 5). In addition to these Epac-mediated functions, we show, for the first time, that Epac-Rap1 signaling is important for regulation of endothelial barrier function.

AJ assembly contributes to the regulation of barrier function. Rap1 is involved in the formation and maintenance of AJ constituted by cadherin (23, 41). Recently, it has been reported that homophilic ligation of E-cadherin induced Rap1 activation, which may be responsible for maturation of AJ (20). Consistently, suppression of endogenous Rap1 inhibits formation of E-cadherin-dependent cell adhesion (36), suggesting the critical role of Rap1 in the establishment of cadherin-based cell-cell contacts. Here, we demonstrate that Rap1 also acts downstream of cAMP-Epac to potentiate VE-cadherin-depen-

dent cell adhesion, thereby improving barrier function. In addition to cAMP-elevating ligands, S1P, which enhances AJ formation and barrier function (18, 26), also activated Rap1 (our unpublished data). Thus, Rap1 may play a crucial role in barrier function induced by various types of barrier-improving factors.

Our data and previous studies show that cAMP protects thrombin-induced endothelial barrier dysfunction. cAMP does not limit the effect of thrombin on the initial loss of endothelial barrier (32). Instead, cAMP enhances the restoration of barrier function disrupted by thrombin. Recently, it was also reported that Cdc42 regulates the restoration of endothelial barrier function disrupted by thrombin (24). Thus, cAMP-Epac-Rap1 signaling may facilitate the formation of VE-cadherin-based cell-cell contacts, cooperatively or in parallel with Cdc42.

Rap1 enhances integrin-dependent cell adhesion in a variety of hematopoietic cells by modulating the affinity and avidity of integrin (6, 22). Cell adhesion to VEC-Fc-coated dishes was augmented by Rap1 activation, suggesting that the homophilic binding of VE-cadherin is also likely ascribed to the affinity and avidity of VE-cadherin modulated by Rap1-triggered inside out signaling. Hogan et al. reported that Rap1 activity is required for the targeting of E-cadherin molecules into nascent cell-cell contact sites, which in turn leads to the maturation of E-cadherin-based cell-cell contacts (20). Thus, cAMP-Epac-Rap1 signaling may also regulate the recruitment of VE-cadherin into maturing cell-cell contacts. Since downstream signaling of Rap1 that increases homophilic binding of VE-cadherin has not yet been characterized, the effector of cAMP-Epac-Rap1 signaling will need to be identified.

The actin cytoskeleton is a critical determinant of vascular integrity (10). PGI2, FSK, and 8-CPT-2′-O-Me-cAMP induced cortical actin rearrangement in a Rap1-dependent manner. FSK-induced VE-cadherin-dependent cell adhesion was inhibited by cytochalasin D. Thus, Rap1 may promote VE-cadherin-dependent cell adhesion by inducing cortical actin rearrangement. AF-6 may act downstream of Rap1 to regulate the actin cytoskeleton, since it binds to GTP-bound Rap1 and the actin cytoskeleton regulator, profilin, and is localized at AJ (2). Consistently, Canoe, the drosophila homolog of AF-6, and Rap1 function in the same molecular pathway during embryonic dorsal closure, which requires cell-cell contacts (3). S1P promotes endothelial barrier function by inducing Rac-dependent cortical actin rearrangement. S1P also induces Rap1 activation (our unpublished data). A previous report indicates that Rac can function downstream of Rap1 in the processing of the amyloid precursor protein (28). Taken together, Rac may act downstream of Rap1 to induce cortical actin rearrangement.

In conclusion, we have demonstrated that the cAMP-Epac-Rap1 signaling pathway promotes VE-cadherin-mediated cell adhesion and consequently improves endothelial barrier function.

ACKNOWLEDGMENTS

We thank J. L. Bos and W. A. Muller for plasmids, M. Matsuda and S. Hattori for adenovirus, J. T. Pearson for critical reading, and M. Sone, K. Yamamoto, and N. Irisawa for technical assistance.

This work was supported by grants from the Ministry of Health, Labor, and Welfare of Japan, from the Promotion of Fundamental Studies in Health Science of the Organization for Pharmaceutical Safety and Research of Japan, from the Ministry of Education, Science, Sports, and Culture of Japan, from the Uehara Memorial Foundation, and from Senri Life Science Foundation.

REFERENCES

1. **Andriopoulou, P., P. Navarro, A. Zanetti, M. G. Lampugnani, and E. Dejana.** 1999. Histamine induces tyrosine phosphorylation of endothelial cell-to-cell adherens junctions. Arterioscler. Thromb. Vasc. Biol. **19**:2286–2297.
2. **Boettner, B., E. E. Govek, J. Cross, and L. Van Aelst.** 2000. The junctional multidomain protein AF-6 is a binding partner of the Rap1A GTPase and associates with the actin cytoskeletal regulator profilin. Proc. Natl. Acad. Sci. USA **97**:9064–9069.
3. **Boettner, B., P. Harjes, S. Ishimaru, M. Heke, H. Q. Fan, Y. Qin, L. Van Aelst, and U. Gaul.** 2003. The AF-6 homolog canoe acts as a Rap1 effector during dorsal closure of the Drosophila embryo. Genetics **165**:159–169.
4. **Bogatcheva, N. V., J. G. Garcia, and A. D. Verin.** 2002. Molecular mechanisms of thrombin-induced endothelial cell permeability. Biochemistry (Moscow) **67**:75–84.
5. **Bos, J. L.** 2003. Epac: a new cAMP target and new avenues in cAMP research. Nat. Rev. Mol. Cell Biol. **4**:733–738.
6. **Bos, J. L., J. de Rooij, and K. A. Reedquist.** 2001. Rap1 signalling: adhering to new models. Nat. Rev. Mol. Cell Biol. **2**:369–377.
7. **Chijiwa, T., A. Mishima, M. Hagiwara, M. Sano, K. Hayashi, T. Inoue, K. Naito, T. Toshioka, and H. Hidaka.** 1990. Inhibition of forskolin-induced neurite outgrowth and protein phosphorylation by a newly synthesized selective inhibitor of cyclic AMP-dependent protein kinase, N-[2-(p-bromocinnamylamino)ethyl]-5-isoquinolinesulfonamide (H-89), of PC12D pheochromocytoma cells. J. Biol. Chem. **265**:5267–5272.
8. **Daly, R. J.** 2004. Cortactin signalling and dynamic actin networks. Biochem. J. **382**:13–25. [Online.] doi:10.1042/BJ20040737.
9. **Dejana, E.** 2004. Endothelial cell-cell junctions: happy together. Nat. Rev. Mol. Cell Biol. **5**:261–270.
10. **Dudek, S. M., and J. G. Garcia.** 2001. Cytoskeletal regulation of pulmonary vascular permeability. J. Appl. Physiol. **91**:1487–1500.
11. **Dudek, S. M., J. R. Jacobson, E. T. Chiang, K. G. Birukov, P. Wang, X. Zhan, and J. G. Garcia.** 2004. Pulmonary endothelial cell barrier enhancement by sphingosine 1-phosphate: roles for cortactin and myosin light chain kinase. J. Biol. Chem. **279**:24692–24700.
12. **Endo, A., K. Nagashima, H. Kurose, S. Mochizuki, M. Matsuda, and N. Mochizuki.** 2002. Sphingosine 1-phosphate induces membrane ruffling and increases motility of human umbilical vein endothelial cells via vascular endothelial growth factor receptor and CrkII. J. Biol. Chem. **277**:23747–23754.
13. **Enserink, J. M., A. E. Christensen, J. de Rooij, M. van Triest, F. Schwede, H. G. Genieser, S. O. Doskeland, J. L. Blank, and J. L. Bos.** 2002. A novel Epac-specific cAMP analogue demonstrates independent regulation of Rap1 and ERK. Nat. Cell Biol. **4**:901–906.
14. **Esser, S., M. G. Lampugnani, M. Corada, E. Dejana, and W. Risau.** 1998. Vascular endothelial growth factor induces VE-cadherin tyrosine phosphorylation in endothelial cells. J. Cell Sci. **111**(Pt 13):1853–1865.
15. **Farmer, P. J., S. G. Bernier, A. Lepage, G. Guillemette, D. Regoli, and P. Sirois.** 2001. Permeability of endothelial monolayers to albumin is increased by bradykinin and inhibited by prostaglandins. Am. J. Physiol. Lung Cell. Mol. Physiol. **280**:L732–L738.
16. **Fukuhara, S., M. J. Marinissen, M. Chiariello, and J. S. Gutkind.** 2000. Signaling from G protein-coupled receptors to ERK5/Big MAPK 1 involves Galpha q and Galpha 12/13 families of heterotrimeric G proteins. Evidence for the existence of a novel Ras AND Rho-independent pathway. J. Biol. Chem. **275**:21730–21736.
17. **Gamble, J. R., J. Drew, L. Trezise, A. Underwood, M. Parsons, L. Kasminkas, J. Rudge, G. Yancopoulos, and M. A. Vadas.** 2000. Angiopoietin-1 is an antipermeability and anti-inflammatory agent in vitro and targets cell junctions. Circ. Res. **87**:603–607.
18. **Garcia, J. G., F. Liu, A. D. Verin, A. Birukova, M. A. Dechert, W. T. Gerthoffer, J. R. Bamberg, and D. English.** 2001. Sphingosine 1-phosphate promotes endothelial cell barrier integrity by Edg-dependent cytoskeletal rearrangement. J. Clin. Investig. **108**:689–701.
19. **Hippenstiel, S., M. Witzenrath, B. Schmeck, A. Hocke, M. Krisp, M. Krull, J. Seybold, W. Seeger, W. Rascher, H. Schutte, and N. Suttorp.** 2002. Adrenomedullin reduces endothelial hyperpermeability. Circ. Res. **91**:618–625.
20. **Hogan, C., N. Serpente, P. Cogram, C. R. Hosking, C. U. Bialucha, S. M. Feller, V. M. M. Braga, W. Birchmeier, and Y. Fujita.** 2004. Rap1 regulates the formation of E-cadherin-based cell-cell contacts. Mol. Cell. Biol. **24**:6690–6700.
21. **Kawasaki, H., G. M. Springett, N. Mochizuki, S. Toki, M. Nakaya, M. Matsuda, D. E. Housman, and A. M. Graybiel.** 1998. A family of cAMP-binding proteins that directly activate Rap1. Science **282**:2275–2279.
22. **Kinbara, K., L. E. Goldfinger, M. Hansen, F. L. Chou, and M. H. Ginsberg.**

2003. Ras GTPases: integrins' friends or foes? Nat. Rev. Mol. Cell Biol. 4:767–776.
23. **Knox, A. L., and N. H. Brown.** 2002. Rap1 GTPase regulation of adherens junction positioning and cell adhesion. Science **295**:1285–1288.
24. **Kouklis, P., M. Konstantoulaki, S. Vogel, M. Broman, and A. B. Malik.** 2004. Cdc42 regulates the restoration of endothelial barrier function. Circ. Res. **94**:159–166.
25. **Langeler, E. G., and V. W. van Hinsbergh.** 1991. Norepinephrine and iloprost improve barrier function of human endothelial cell monolayers: role of cAMP. Am. J. Physiol. **260**:C1052–C1059.
26. **Lee, M. J., S. Thangada, K. P. Claffey, N. Ancellin, C. H. Liu, M. Kluk, M. Volpi, R. I. Sha'afi, and T. Hla.** 1999. Vascular endothelial cell adherens junction assembly and morphogenesis induced by sphingosine-1-phosphate. Cell **99**:301–312.
27. **Lum, H., H. A. Jaffe, I. T. Schulz, A. Masood, A. RayChaudhury, and R. D. Green.** 1999. Expression of PKA inhibitor (PKI) gene abolishes cAMP-mediated protection to endothelial barrier dysfunction. Am. J. Physiol. **277**: C580–C588.
28. **Maillet, M., S. J. Robert, M. Cacquevel, M. Gastineau, D. Vivien, J. Bertoglio, J. L. Zugaza, R. Fischmeister, and F. Lezoualc'h.** 2003. Crosstalk between Rap1 and Rac regulates secretion of sAPPalpha. Nat. Cell Biol. **5**:633–639.
29. **Miles, A. A., and E. M. Miles.** 1952. Vascular reactions to histamine, histamine-liberator and leukotaxine in the skin of guinea-pigs. J. Physiol. **118**: 228–257.
30. **Mochizuki, N., Y. Ohba, E. Kiyokawa, T. Kurata, T. Murakami, T. Ozaki, A. Kitabatake, K. Nagashima, and M. Matsuda.** 1999. Activation of the ERK/MAPK pathway by an isoform of rap1GAP associated with G alpha(i). Nature **400**:891–894.
31. **Mori, Y., T. Nishikimi, N. Kobayashi, H. Ono, K. Kangawa, and H. Matsuoka.** 2002. Long-term adrenomedullin infusion improves survival in malignant hypertensive rats. Hypertension **40**:107–113.
32. **Moy, A. B., J. E. Bodmer, K. Blackwell, S. Shasby, and D. M. Shasby.** 1998. cAMP protects endothelial barrier function independent of inhibiting MLC20-dependent tension development. Am. J. Physiol. **274**:L1024–L1029.
33. **Navarro, P., L. Ruco, and E. Dejana.** 1998. Differential localization of VE- and N-cadherins in human endothelial cells: VE-cadherin competes with N-cadherin for junctional localization. J. Cell Biol. **140**:1475–1484.
34. **Ohba, Y., K. Ikuta, A. Ogura, J. Matsuda, N. Mochizuki, K. Nagashima, K. Kurokawa, B. J. Mayer, K. Maki, J. Miyazaki, and M. Matsuda.** 2001. Requirement for C3G-dependent Rap1 activation for cell adhesion and embryogenesis. EMBO J. **20**:3333–3341.
35. **Parandoosh, Z., C. A. Bogowitz, and M. P. Nova.** 1998. A fluorometric assay for the measurement of endothelial cell density in vitro. In Vitro Cell. Dev. Biol. Anim. **34**:772–776.
36. **Price, L. S., A. Hajdo-Milasinovic, J. Zhao, F. J. Zwartkruis, J. G. Collard, and J. L. Bos.** 2004. Rap1 regulates E-cadherin-mediated cell-cell adhesion. J. Biol. Chem. **279**:35127–35132.
37. **Quilliam, L. A., H. Mueller, B. P. Bohl, V. Prossnitz, L. A. Sklar, C. J. Der, and G. M. Bokoch.** 1991. Rap1A is a substrate for cyclic AMP-dependent protein kinase in human neutrophils. J. Immunol. **147**:1628–1635.
38. **Shaywitz, A. J., and M. E. Greenberg.** 1999. CREB: a stimulus-induced transcription factor activated by a diverse array of extracellular signals. Annu. Rev. Biochem. **68**:821–861.
39. **Stelzner, T. J., J. V. Weil, and R. F. O'Brien.** 1989. Role of cyclic adenosine monophosphate in the induction of endothelial barrier properties. J. Cell. Physiol. **139**:157–166.
40. **Ukropec, J. A., M. K. Hollinger, S. M. Salva, and M. J. Woolkalis.** 2000. SHP2 association with VE-cadherin complexes in human endothelial cells is regulated by thrombin. J. Biol. Chem. **275**:5983–5986.
41. **Yajnik, V., C. Paulding, R. Sordella, A. I. McClatchey, M. Saito, D. C. Wahrer, P. Reynolds, D. W. Bell, R. Lake, S. van den Heuvel, J. Settleman, and D. A. Haber.** 2003. DOCK4, a GTPase activator, is disrupted during tumorigenesis. Cell **112**:673–684.
42. **Yano, H., Y. Mazaki, K. Kurokawa, S. K. Hanks, M. Matsuda, and H. Sabe.** 2004. Roles played by a subset of integrin signaling molecules in cadherin-based cell-cell adhesion. J. Cell Biol. **166**:283–295.
43. **Yuan, S. Y.** 2002. Protein kinase signaling in the modulation of microvascular permeability. Vascul. Pharmacol. **39**:213–223.

The EMBO Journal (2005) 24, 325–335 | © 2005 European Molecular Biology Organization | All Rights Reserved 0261-4189/05
www.embojournal.org

THE EMBO JOURNAL

Identification of neuromedin S and its possible role in the mammalian circadian oscillator system

Kenji Mori[1], Mikiya Miyazato[1], Takanori Ida[2], Noboru Murakami[2], Ryota Serino[3], Yoichi Ueta[3], Masayasu Kojima[4] and Kenji Kangawa[1,*]

[1]Department of Biochemistry, National Cardiovascular Center Research Institute, Fujishirodai, Suita, Osaka, Japan, [2]Department of Veterinary Physiology, Faculty of Agriculture, University of Miyazaki, Miyazaki, Japan, [3]Department of Physiology, School of Medicine, University of Occupational and Environmental Health, Kitakyushu, Fukuoka, Japan and [4]Division of Molecular Genetics, Institute of Life Science, Kurume University, Kurume, Fukuoka, Japan

The discovery of neuropeptides has resulted in an increased understanding of novel regulatory mechanisms of certain physiological phenomena. Here we identify a novel neuropeptide of 36 amino-acid residues in rat brain as an endogenous ligand for the orphan G protein-coupled receptor FM-4/TGR-1, which was identified to date as the neuromedin U (NMU) receptor, and designate this peptide 'neuromedin S (NMS)' because it is specifically expressed in the suprachiasmatic nuclei (SCN) of the hypothalamus. NMS shares a C-terminal core structure with NMU. The NMS precursor contains another novel peptide. NMS mRNA is highly expressed in the central nervous system, spleen and testis. In rat brain, NMS expression is restricted to the core of the SCN and has a diurnal peak under light/dark cycling, but remains stable under constant darkness. Intracerebroventricular administration of NMS in rats activates SCN neurons and induces nonphotic type phase shifts in the circadian rhythm of locomotor activity. These findings suggest that NMS in the SCN is implicated in the regulation of circadian rhythms through autocrine and/or paracrine actions.

The EMBO Journal (2005) **24**, 325–335. doi:10.1038/sj.emboj.7600526; Published online 6 January 2005
Subject Categories: signal transduction; neuroscience
Keywords: circadian rhythm; endogenous ligand; neuropeptide; orphan G protein-coupled receptor; suprachiasmatic nucleus

Introduction

G protein-coupled receptors (GPCRs) constitute a large protein superfamily, and share the seven-transmembrane motif as common structure. The progress of human genome sequencing has revealed the existence of several hundred orphan GPCRs, for which ligands have not yet been identified (Vassilatis *et al*, 2003). GPCRs play crucial roles in cell-to-cell communication involved in a variety of physiological phenomena, and are the most common target of pharmaceutical drugs. Therefore, identification of endogenous ligands for orphan GPCRs will lead to clarification of novel regulatory mechanisms of physiological phenomena and to novel drug targets. Recently, many bioactive molecules have been discovered or identified as endogenous ligands of orphan GPCRs using a reverse-pharmacological technique (Civelli *et al*, 2001).

Neuromedin U (NMU), initially isolated from porcine spinal cord by our group, is a brain-gut neuropeptide that has a potent activity to cause uterine smooth muscle contraction (Minamino *et al*, 1985). The physiological roles of NMU in the central nervous system (CNS) have been poorly understood, because the NMU receptor in the CNS has not been identified. In contrast, the peripheral activities of NMU have been well characterized; these include contraction of smooth muscle (Minamino *et al*, 1985), elevation of arterial blood pressure (Minamino *et al*, 1985), alternation of intestinal ion transport (Brown and Quito, 1988) and control of local blood flow (Sumi *et al*, 1987; Gardiner *et al*, 1990). Recently, NMU was identified as an endogenous ligand for two orphan GPCRs, FM-3/GPR66 and FM-4/TGR-1, which were then designated the NMU receptors type-1 (NMU1R) and type-2 (NMU2R), respectively (Fujii *et al*, 2000; Hedrick *et al*, 2000; Hosoya *et al*, 2000; Howard *et al*, 2000; Kojima *et al*, 2000; Raddatz *et al*, 2000). The FM-3/GPR66 mRNA exhibits wide distribution in peripheral tissues. In contrast, the FM-4/TGR-1 mRNA is mainly expressed in the CNS, especially in the hypothalamic paraventricular nucleus (PVN). These reports have provided novel insights into the function of NMU in the CNS. The central NMU suppresses feeding (Howard *et al*, 2000; Kojima *et al*, 2000), regulates energy homeostasis (Nakazato *et al*, 2000; Hanada *et al*, 2003), affects the cardiovascular system (Chu *et al*, 2002) and induces the release of stress-mediating molecules (Hanada *et al*, 2001; Ozaki *et al*, 2002; Wren *et al*, 2002). Our detailed analysis by RT–PCR recently demonstrated that the FM-4/TGR-1 mRNA is expressed not only in the PVN but also in the suprachiasmatic nucleus (SCN) of the hypothalamus (Nakahara *et al*, 2004). However, the functional role of FM-4/TGR-1 in the SCN remains unclear.

The SCN is the site of the master circadian pacemaker in mammals, which governs the circadian rhythm of behavioral and physiological processes. The pacemaker generates the near-24-h period of the circadian rhythm by an autoregulatory transcription/translation feedback loop composed of clock-gene families of transcription factors, and is entrained to the 24-h daily cycle by periodic environmental cues, such as light/dark cycle and temperature, which are typical examples of photic and nonphotic signals, respectively (Lowrey and Takahashi, 2000; Reppert and Weaver, 2001, 2002). The SCN is functionally and anatomically divided into 'core' and 'shell' regions, which correspond to the ventrolateral and dorsomedial portions of the SCN, respectively (Moore *et al*,

*Corresponding author. Department of Biochemistry, National Cardiovascular Center Research Institute, 5-7-1 Fujishirodai, Suita, Osaka 565-8565, Japan. Tel.: +81 6 6833 5012; Fax: +81 6 6835 5402; E-mail: kangawa@ri.ncvc.go.jp

Received: 5 July 2004; accepted: 26 November 2004; published online: 6 January 2005

2002). The SCN core and shell play roles in circadian entrainment and spontaneous generation of strong rhythm, respectively (Hamada *et al*, 2001). Several neuropeptides participate in the regulation of the circadian pacemaker within the SCN (Reppert and Weaver, 2001). For example, vasoactive intestinal polypeptide (VIP), which is expressed in the SCN core, plays roles in both photic entrainment and maintenance of the circadian rhythm within the SCN (Piggins and Cutler, 2003). Therefore, the expression of FM-4/TGR-1 within the SCN strongly suggests that the endogenous ligand for its receptor is involved in the circadian oscillator system.

Based on the sequences obtained by a homology search of genomic and expressed sequence tag (EST) databases with known GPCR, our group independently identified FM-4/TGR-1 as an orphan GPCR, and have searched for its endogenous ligand. Here we report the identification of a novel neuropeptide, neuromedin S (NMS), which was purified from rat brain extracts as an endogenous ligand for FM-4/TGR-1 using a reverse-pharmacological technique. The NMS mRNA is specifically and rhythmically expressed in the SCN core in rat brain with a diurnal peak. Intracerebroventricular (ICV) administration of NMS in rats activates SCN neurons and causes nonphotic type phase shifts in the circadian rhythm of locomotor activity. Our data suggest that NMS is a candidate for a nonphotic entrainment factor of circadian rhythm and that NMS acts through its receptor in an autocrine and/or paracrine manner within the SCN.

Results

Purification of NMS

To identify endogenous ligands for orphan GPCRs, we have purified natural peptides from tissue extracts using a reverse-pharmacological technique (Kojima *et al*, 1999, 2000). While searching for endogenous ligands of the orphan GPCR FM-4/TGR-1 (identified to date as NMU2R), gel filtration of rat brain extracts revealed two agonist activities capable of increasing intracellular calcium ion concentration ($[Ca^{2+}]_i$) in CHO cells expressing FM-4/TGR-1 (Figure 1A, P1 and P2). P2 activity was eluted in fractions with a relative molecular mass (M_r) of 2500, corresponding to the M_r of rat NMU (2642.9), and NMU was purified from these fractions (data not shown). In contrast, P1 activity was found at a larger M_r (~4000) by gel filtration chromatography and was more hydrophobic by reverse-phase HPLC (RP-HPLC) compared to P2 activity, indicating that the rat brain contains another endogenous ligand for FM-4/TGR-1. Therefore, P1 activity was purified to homogeneity by successive HPLC steps (Figure 1B, upper panel). The final yield of the purified peptide was approximately 2.5 pmol from 420 rat brains (510 g).

Structure determination of NMS

The partial N-terminal amino-acid sequence of the purified peptide was determined by a protein sequencer to be LPRLLHTDSRMATIDFPKK. To elucidate the complete amino-acid sequence of this peptide, human, rat and mouse cDNAs encoding the purified peptide were isolated from the brain of each species by PCR. The rat cDNA encoded a 152-residue protein containing features characteristic of an N-terminal signal peptide (von Heijne, 1986) (Figure 2A). This preproprotein contained four potential processing sites to be cleaved by subtilisin-like proprotein convertases

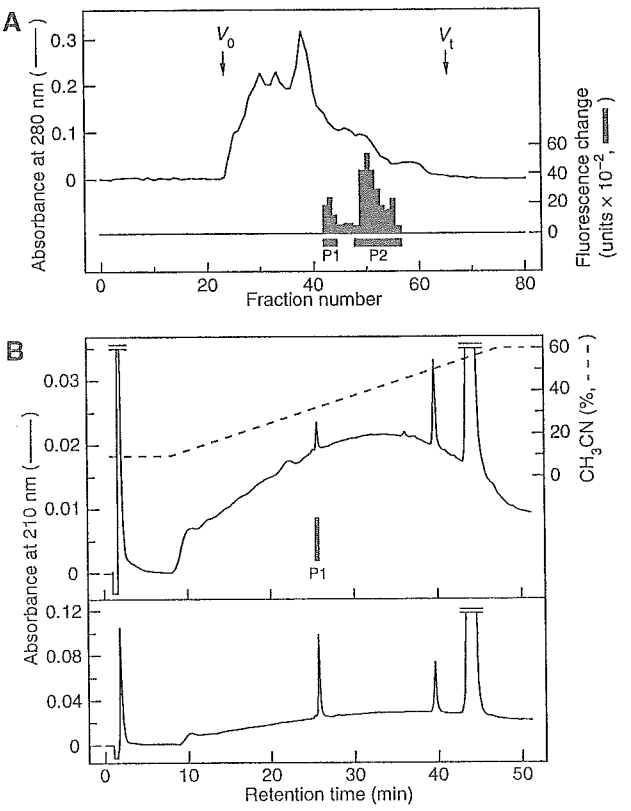

Figure 1 Purification of NMS. (**A**) Gel filtration on a Sephadex G-50 (fine) column of the SP-III fraction from 510 g of rat brain. Black bars indicate fluorescence change due to $[Ca^{2+}]_i$ increase in CHO/FM-4. Active fractions containing NMS (P1) and NMU (P2) are indicated. V_0, void volume; V_t, total volume. (**B**) Chromatographic comparison using RP-HPLC of natural NMS (upper panel) and synthetic NMS (lower panel). The black bar indicates $[Ca^{2+}]_i$-increasing activity (upper panel). Each peptide was applied to a Chemcosorb 3ODS-H column. The flow rate was 0.2 ml/min. Solvent system, a linear gradient elution from (A) to (B) for 40 min. H_2O:CH_3CN:10% TFA for (A) was 90:10:1, for (B) 40:60:1 (v/v).

(Rouille *et al*, 1995). The N-terminal sequence of the purified peptide directly followed the third processing site, indicating that the purified peptide is generated by cleavage at the third and fourth sites. The fourth processing site contained Gly 145, which presumably serves as an amide donor for C-terminal amidation (Rouille *et al*, 1995). All characteristic structures described above were conserved in the preproproteins of human and mouse. We therefore deduced the primary structure of the newly purified peptide to be LPRLLHTDSRMATIDFPKKDPTTSLGRPFFLFRPRN-NH_2, and designated this 36-residue peptide NMS. Mass spectrometric analysis revealed that the observed monoisotopic *m/z* value of the purified peptide (4240.2) was very close to the theoretically predicted value for rat NMS (4240.3). Moreover, the synthetic NMS had an identical retention time to the natural peptide on RP-HPLC (Figure 1B), suggesting that the deduced primary structure is identical to that of the natural peptide. The N-terminal portion of NMS has no sequence homology to previously known peptides or proteins. On the other hand, the C-terminal amidated seven-residue sequence of NMS is identical to that of NMU (Minamino *et al*, 1985) (Figure 2B); this sequence has been found to be essential for NMU receptor binding (Minamino *et al*, 1985). NMS is not a splice

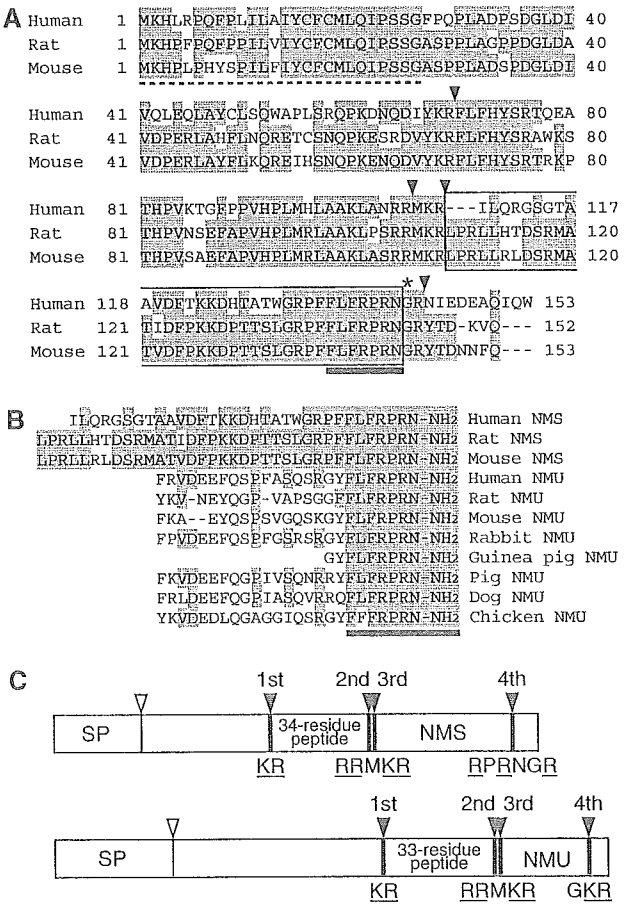

Figure 2 Structure of NMS. (**A**) Amino-acid sequences of human, rat and mouse prepro-NMS. Identical residues are shaded. The dotted line denotes the predicted signal peptide. The arrowheads indicate proteolytic processing sites. The asterisk shows a glycine residue, which serves as an amide donor for C-terminal amidation. NMS sequences are boxed. Sequences conserved between NMS and NMU are indicated by a solid underline. The sequence data for the human, rat and mouse NMS cDNAs have been submitted to the DDBJ/EMBL/GenBank databases under accession nos. AB164464, AB164465 and AB164466, respectively. (**B**) Sequence comparison of NMS and NMU. Human, rat and mouse NMS and NMU sequences are aligned. Residues identical between peptides are shaded. Conserved core sequences are indicated by a solid underline. (**C**) Schematic representation of the preproproteins of rat NMS and NMU. The preproproteins of NMS and NMU are represented by boxes divided into protein domain, proportional to their length. The open and filled arrowheads indicate cleavage sites by signal peptidase and proprotein convertase, respectively. The sequences of the proteolytic processing sites are shown. The basic amino-acid residues recognized by proprotein convertase are underlined. SP, signal peptide.

variant of NMU, because the human *NMS* and *NMU* genes were mapped to chromosomes 2q11.2 and 4q12, respectively, by a blast search of the genome database. The structural organization and putative promoter region of the *NMS* gene were also analyzed computationally (see Supplementary data and Supplementary Figure S1). The four proteolytic processing sites described above in the NMS proprotein are conserved in the NMU proprotein (Lo *et al*, 1992) (Figure 2C), and the amino-acid sequences between the first and second processing sites show high homology to each other, indicating the existence of other novel 34- and 33-residue neuropeptides produced from the NMS and NMU proproteins, respectively, by processing at the first and second sites.

Pharmacological characterization of NMS

Because NMS and NMU share a core structure that is required for binding to receptors, the interaction of NMS with FM-3/GPR66 and FM-4/TGR-1 was examined using synthetic peptides. Human NMS induced dose-dependent, robust increases in $[Ca^{2+}]_i$ in CHO cells expressing either FM-3/GPR66 or FM-4/TGR-1 (CHO/FM-3 or CHO/FM-4, respectively), with half-maximal response concentrations (EC_{50}) of 6.5×10^{-11} and 9.1×10^{-11} M, respectively (Figure 3A and B). Rat NMS and NMU, and human NMU also showed comparable potency and efficacy for these receptors. Neither NMS nor NMU induced a response in CHO cells transfected with vector alone (data not shown). Competitive radioligand binding analysis showed high-affinity binding of NMS to receptors. Binding of [^{125}I-Tyr^0]-human NMS to FM-3/GPR66 was qinhibited in a dose-dependent manner by human NMS and NMU, with similar inhibition constants (IC_{50}) of 1.2×10^{-9} M (Figure 3C). On the other hand, human NMS had a higher binding affinity to FM-4/TGR-1 than did NMU ($IC_{50} = 1.0 \times 10^{-10}$ and 6.8×10^{-10} M, respectively) (Figure 3D). These data indicate that NMS, as well as NMU, is a cognate ligand for both FM-3/GPR66 and FM-4/TGR-1.

In addition, the activities of NMS and NMU were compared in chick rectum contraction and rat systemic blood pressure assays. NMS induced contraction of chick rectum and elevation of rat systemic blood pressure with activities similar to NMU (see Supplementary Figure S2).

Expression analysis of NMS

We investigated the tissue distribution of the NMS mRNA in various rat tissues using quantitative RT–PCR. The NMS mRNA was expressed mainly in the CNS, spleen and testis (Figure 4A). The highest level of NMS gene expression was found in the hypothalamus. Interestingly, the NMS mRNA was expressed predominantly in the SCN, with only very slight expression in other brain regions (Figure 4B). *In situ* hybridization histochemistry also showed that the NMS mRNA expression was restricted to the SCN in the rat brain (Figure 4C). No hybridization signal was observed in other brain regions. In the rat, the SCN is divided into core, where the neuropeptide VIP is expressed, and shell, where the neuropeptide arginine vasopressin (AVP) is expressed (Moore *et al*, 2002). The NMS mRNA was expressed in the SCN core (Figure 4D–F), in a similar manner to the VIP mRNA. This unique expression pattern of NMS in the brain and peripheral tissues led us to speculate that NMS may play important roles in tissue-specific physiological functions, such as circadian rhythm regulation in the SCN, immune response in the spleen and spermatogenesis in the testis. We thus examined the possible role of NMS in the circadian oscillation systems of the SCN.

Expression pattern of NMS within the SCN

We examined the time-dependent profile of the NMS mRNA expression in the rat SCN. Under 12-h light/dark cycles, a pronounced rhythmic expression of the NMS mRNA was observed (ANOVA, $F_{(3,10)} = 11.287$, $P < 0.005$), with the largest decrease occurring during the dark period, followed by a gradual increase until the late light period at ZT11 (Zeitgeber time, ZT; ZT0 is lights on and ZT12 is lights off) (Figure 5A). Under conditions of constant darkness, no NMS mRNA

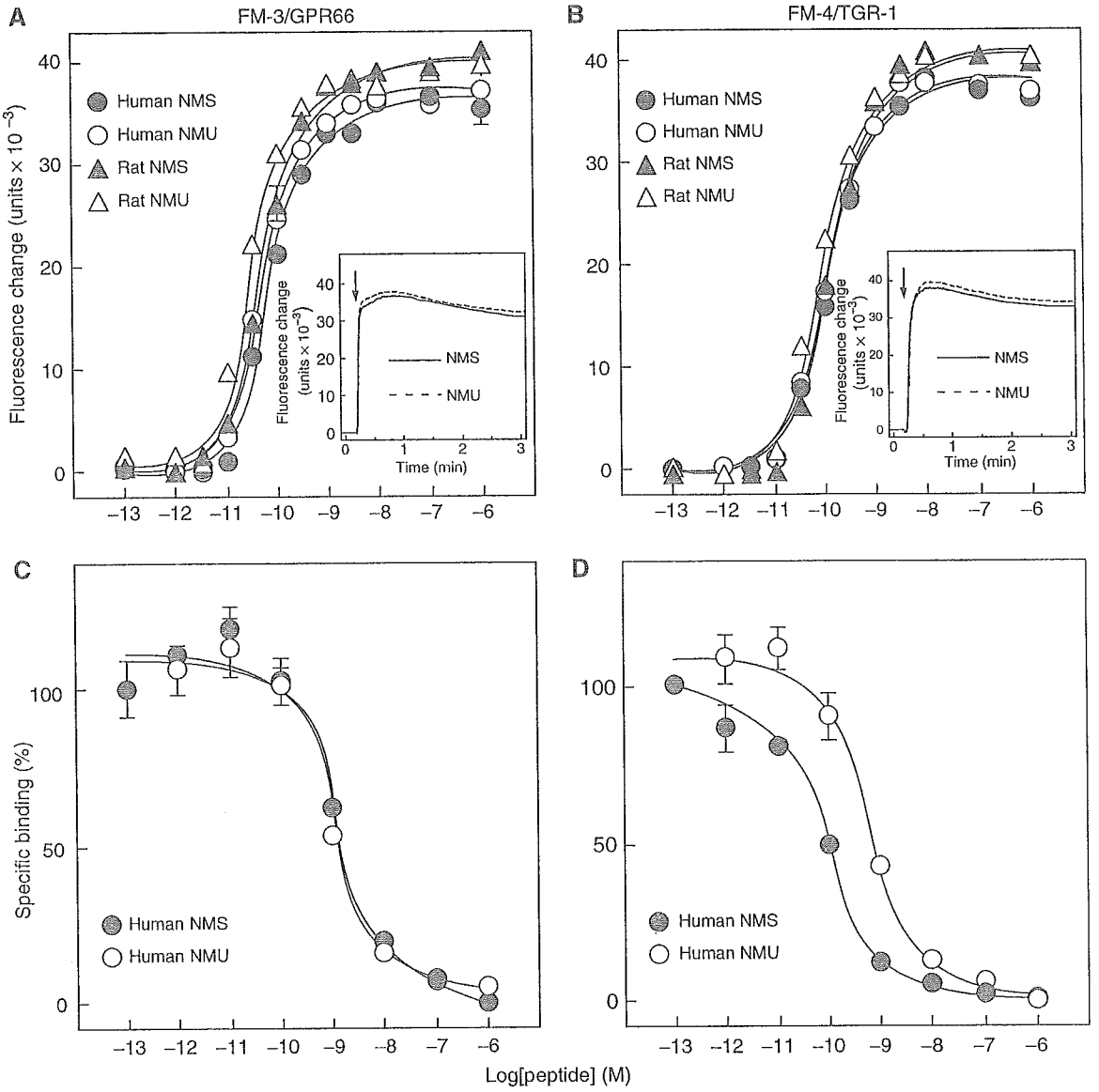

Figure 3 Pharmacological characterization of synthetic NMS using human FM-3/GPR66 and FM-4/TGR-1 stably expressed in CHO cells. (**A, B**) Dose-response relationships of $[Ca^{2+}]_i$ change for human NMS (filled circle), human NMU (open circle), rat NMS (filled triangle) and rat NMU (open triangle) in CHO/FM-3 (A) and CHO/FM-4 (B) cells. Data points are means±s.e.m. of triplicates for each experiment. Insets show the time course of $[Ca^{2+}]_i$ changes induced by human NMS (solid line) and human NMU (dotted line). Each peptide (10^{-8} M) was added at the time indicated by the arrow. (**C, D**) Competitive radioligand binding analysis. [^{125}I-Tyr^0]-human NMS binding to FM-3/GPR66 (C) and FM-4/TGR-1 (D) was displaced by increasing concentrations of human NMS (filled circle) and human NMU (open circle). Data were determined in triplicate.

oscillation was observed (ANOVA, $F_{(3,11)}=1.170$, $P>0.3$) (Figure 5B). These data indicate that the expression of NMS is not under the control of clock-gene families that generate circadian rhythm by an autoregulatory transcription/translation feedback loop (Lowrey and Takahashi, 2000; Reppert and Weaver, 2001, 2002). We next examined the NMS mRNA level within the SCN in response to a light pulse under conditions of constant darkness. The expression of the NMS mRNA was significantly decreased 1 h after the light exposure at CT6 (circadian time, CT; CT0–12 is subjective day and CT12–24 is night) (Figure 5C). We also assessed the effect of a dark pulse on NMS expression within the SCN of rats maintained under light/dark cycling. When rats were exposed to a dark pulse at ZT6, the NMS mRNA level tended to be suppressed (Figure 5D).

Intracerebroventricularly administered NMS induces phase shifts in the circadian rhythm of locomotor activity

In the SCN, two types of receptors for NMS were expressed, although the FM-4/TGR-1 mRNA was more highly expressed than the FM-3/GPR66 mRNA (23.78±2.61 and 0.27±0.006 copies/ng of total RNA, respectively). We therefore examined the effect of ICV administration of NMS on the circadian rhythm of locomotor activity in rats maintained under constant darkness. When injected at CT3–9, 1 nmol of rat NMS phase-advanced the rhythm of locomotor activity (Figure 6A and E), whereas administration at CT22–24 induced a phase delay (Figure 6D and E). No phase-shifting effect was observed during either early or middle subjective night (Figure 6B, C and E). The phase-response curve (PRC) for NMS

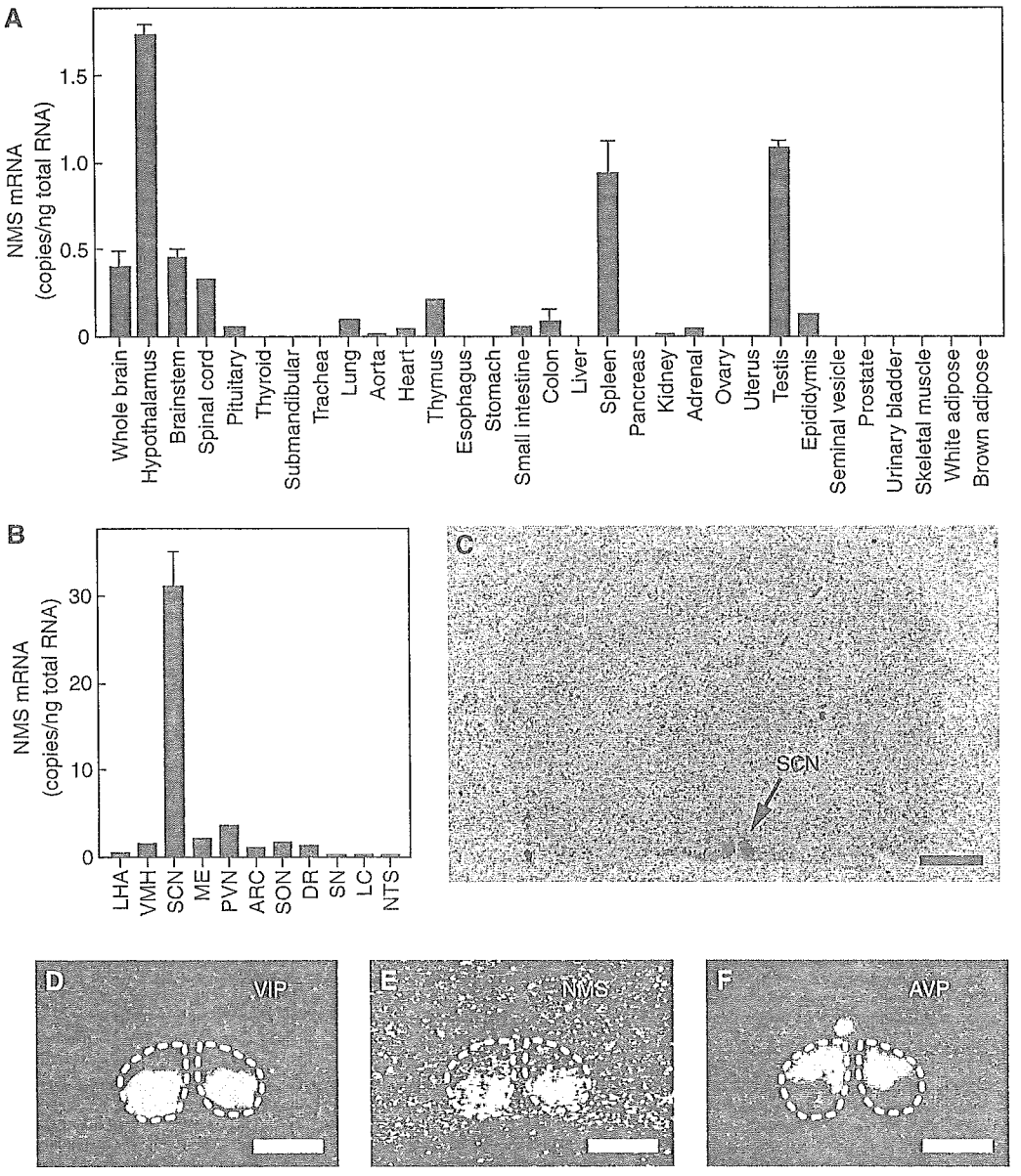

Figure 4 Expression studies of rat NMS. (**A, B**) Quantitative RT–PCR analysis of the NMS mRNA in a rat multiple-tissue cDNA panel. Each column represents the mean±s.e.m. of triplicate experiments. LHA, lateral hypothalamic area; VMH, ventromedial hypothalamus; SCN, suprachiasmatic nucleus; ME, median eminence; PVN, paraventricular nucleus; ARC, arcuate nucleus; SON, supraoptic nucleus; DR, dorsal raphe; SN, substantia nigra; LC, locus coeruleus; NTS, nucleus of the solitary tract. (**C**) Autoradiogram of the NMS mRNA expression in a coronal section of the rat brain. Scale bar, 2 mm. (**D–F**) Distribution of VIP (D), NMS (E) and AVP (F) mRNA in the rat SCN. Serial sections were used. The SCN is indicated with a dotted line. Scale bar, 500 μm.

fluctuated significantly (ANOVA, $F_{(14,28)}=2.549$, $P<0.05$). These effects were dependent on both phase and dose (Figure 6E and F). Saline administration did not elicit a phase shift under the same conditions (data not shown). Circadian period length was not influenced by ICV administration of NMS at any time. In addition, after ICV administration of NMS, the expression of c-Fos protein, a marker of neuronal activation, was increased within the SCN compared with saline-administered control rats (Figure 6G and H). The c-Fos protein was preferentially expressed on the core of the SCN. To further test the effects of NMS on SCN function, NMS was microinjected directly into the SCN. Intranuclearly administered NMS also induced phase advance and delay in the circadian rhythm of locomotor activity at CT6 and CT23, respectively (see Supplementary Figure S3). Saline administration had no effect. Taken together, these data suggest that endogenous NMS acts through its receptors to have a strong effect on SCN function.

Discussion

In this study, we have purified a novel neuropeptide, NMS, as an endogenous ligand for the orphan GPCR FM-4/TGR-1 (designated to date as NMU2R). Pharmacological characterization using recombinant receptors showed that NMS is a cognate ligand for both FM-3/GPR66 and FM-4/TGR-1, indicating that NMS shares these receptors with NMU, which is a brain-gut neuropeptide originally isolated from porcine